This is a preprint, the final version is subject to change, of the American Mineralogist (MSA)
Cite as Authors (Year) Title. American Mineralogist, in press.
DOI: https://doi.org/10.2138/am-2018-6199

1 **Revision 3**

# 2 New petrological, geochemical and geochronological perspectives 3 on andesite-dacite magma genesis at Ruapehu volcano, New 4 Zealand

5

6

7 Chris E. Conway[1,2]*, John A. Gamble[1,3], Colin J. N. Wilson[1], Graham S. Leonard[4], Dougal
8 B. Townsend[4], Andrew T. Calvert[5]

9

10

11 [1] School of Geography, Environment and Earth Sciences, Victoria University, PO Box 600,
12 Wellington 6140, New Zealand

13 [2] Department of Geology and Paleontology, National Museum of Nature and Science, 4-1-1
14 Amakubo, Tsukuba, Ibaraki 305-0005, Japan

15 [3] School of Biological, Earth and Environmental Sciences, University College Cork, Ireland

16 [4] GNS Science, PO Box 30-368, Lower Hutt 6315, New Zealand

17 [5] US Geological Survey, 345 Middlefield Road, MS-937, Menlo Park, CA 94025, USA

18

19

20 *Email: chrisconway@kahaku.go.jp

This is a preprint, the final version is subject to change, of the American Mineralogist (MSA)
Cite as Authors (Year) Title. American Mineralogist, in press.
DOI: https://doi.org/10.2138/am-2018-6199


## ABSTRACT

Time-composition relationships in eruptive sequences at composite volcanoes can show how the ongoing intrusion of magmas progressively affects the lithosphere at continental convergent margins. Here, new whole-rock and microanalytical major and trace element data from andesite-dacite lava flows are integrated with previous studies and existing isotopic data, and placed within the framework of a high-resolution chronostratigraphy for Ruapehu volcano (southern Taupo Volcanic Zone, New Zealand). The geochemical evolution of lavas erupted over the ~200 kyr lifetime of the exposed edifice reflects variable degrees of fractionation and systematic changes in the type of crustal assimilation in the Ruapehu magma system. Lavas erupted from ~200–150 ka have previously been distinguished from those erupted <150 ka based on Sr-Nd isotopic characteristics, which indicate that the oldest lavas were sourced from magmas that assimilated oceanic crust. Such source rocks underlie the regionally widespread Mesozoic meta-sedimentary greywacke-argillite basement, which was conversely assimilated by <150 ka magmas. New results from this work reveal that since 150 ka, an upper limit of magma differentiation occurred from ~50–35 ka. High $K_2O$ (~6 wt. %) and Rb contents (~270 ppm) in melt inclusions, interstitial glass, and glass from *in situ* quenched melts of partially fused crustal xenoliths are reported for andesite-dacite lavas erupted during this period. In addition to crystal fractionation, selective partial melting and assimilation of K-and Rb-rich mineral phases (e.g. biotite, K-feldspar) that are significant components of the meta-sedimentary basement rocks is inferred to explain these geochemical characteristics. These processes coincided also with the effusion of high-MgO andesite-dacite lavas that display petrological evidence for mixing between andesite-dacite and more mafic magmas. An influx of hotter mafic magma into the system explains why the extent of crustal assimilation recorded by Ruapehu lavas peaked during the ~50–35 ka eruptive period. From 26 ka to the present, andesite lavas have reverted to more mafic compositions with less

potassic melt inclusion and whole-rock compositions when compared to the ~50–35 ka lavas. We suggest that the younger lavas assimilated less-enriched melts because fertile phases had been preferentially extracted from the crustal column during earlier magmatism. This scenario of bottom-up heating of the lithosphere and exhaustion of fertile phases due to the progressive intrusion of magma explains the geochemical evolution of Ruapehu lavas. This model may be applicable to other long-lived composite volcanoes of the circum-Pacific continental arcs.

**Keywords:** Ruapehu; andesite; dacite; petrogenesis; arc magma; crustal contamination; high-Mg andesite

## INTRODUCTION

The compositional ranges of eruptive products generated at continental arc volcanoes often display linear compositional arrays that extend from basalt to dacite and, occasionally, rhyolite (e.g. Hildreth et al. 2003; Price et al. 2005; Hora et al. 2007; Singer et al. 2008; Hildreth and Fierstein 2012). The time-sequenced geochemical variations of eruptive products are typically non-systematic, however, and do not necessarily reflect the long-term evolution of a common magma source by simple progressive fractionation and assimilation (cf. Eichelberger et al. 2006). The timescales of compositional heterogeneity specified by the products of short-lived eruptive episodes (<1–20 yr; e.g. Clynne 1999; Coombs et al. 2000, 2013) or preserved in lava flow sequences (1–10 kyr; Gamble et al. 1999, 2003; Dungan et al. 2001; Frey et al. 2004), indicate that magmas with diverse parentage are generated and erupted relatively frequently. As such, compositional variations within lava flow sequences are likely to reflect the eruption of discrete batches of magma that have followed unique

pathways of differentiation in the crust (e.g. Hobden et al. 1999; Gamble et al. 2003; Frey et al. 2004; Eichelberger et al. 2006; Sisson et al. 2013).

Beneath arc volcanoes, the processes of crustal anatexis, magma mixing, and crystal fractionation are the primary agents of magma differentiation (e.g. Price et al. 2012; Kent 2013; Lee and Bachmann 2014). Two commonly documented signatures of intermediate arc magmas that arise from these processes are: (a) the generation and entrapment of melts that are substantially more silicic than their host whole-rock compositions (see compilations by Reubi and Blundy 2009; Kent 2013), and (b) disequilibrium petrographic textures that reflect mixing between felsic and mafic components and their crystal cargoes, together with evolving intensive parameters such as pressure, temperature and degassing (e.g. Clynne 1999; Dungan and Davidson 2004; Kent et al. 2010; Koleszar et al. 2012). Because the felsic and mafic end-members seldom erupt independently at composite volcanoes, their cryptic existence within crustal magma systems is recorded within mineral-hosted melt inclusions and interstitial glass (e.g. Reubi and Blundy 2008) and the crystal cargo of the derivative intermediate composition magmas (e.g. Eichelberger 1975; Streck et al. 2007). Thus, the nature and origin of felsic and mafic sources, and the processes by which they interact, may be elucidated by microanalytical investigations (Davidson et al. 2007). Constraining these magma sources and the subsequent mixing parameters and processes is critical to understanding the assembly of arc magmas.

Compositions of eruptive products from arc volcanoes record not only snapshots of crustally dominated magma processes, but also the cumulative effect of progressive heating and "conditioning" of the lower, middle, and upper crust in response to the magmas that have passed through these regions. How magmatic sources and processes vary throughout time and what controls those variations represent fundamental questions for understanding petrogenesis at and the eruption potential of arc volcanoes. Critical to addressing these

questions is the collection of high-resolution eruptive histories for arc volcanoes that are constrained by field studies and radiometric age data so that eruptive products can be accurately sequenced (e.g. Dungan et al. 2001; Frey et al. 2004). Here, we apply this approach to Ruapehu volcano in the southern Taupo Volcanic Zone (TVZ; New Zealand). We combine a revised chronostratigraphy of Ruapehu volcano (Conway et al. 2016) with detailed geochemical sequencing of lava flow compositions in order to investigate the genesis of andesite-dacite magmas at this volcano throughout the ~200 kyr lifetime of the exposed edifice.

## GEOLOGICAL SETTING

The Taupo Volcanic Zone (TVZ; Fig. 1) is a zone of continental magmatism in the North Island of New Zealand related to the subduction of the Pacific Plate beneath the Australian Plate (Cole 1990). The basement geology of the TVZ comprises greywacke-argillite meta-sedimentary rocks of the Torlesse Terrane, which are exposed to the east of the volcanic area (Adams et al. 2009; Fig. 1). Waipapa Terrane meta-sedimentary rocks crop out to the west of the TVZ (Fig. 1), but are not considered to play a significant role in TVZ magmatism (e.g. Price et al. 2015). Caldera-forming rhyolitic eruptions have dominated the style of volcanic activity within the TVZ for 2 Myr, however, the northern and southern extents of the rifted arc are marked by the active andesite-dacite stratovolcanoes of White Island and Ruapehu (Wilson et al. 1995; Fig. 1).

Ruapehu volcano is a ~150 $km^3$ complex composite edifice primarily composed of stacked sequences of lava flows and associated breccias, intercalated with till and subsidiary volumes of proximal pyroclastic flow and fall deposits (Hackett and Houghton 1989). The exposed edifice has a lifetime of ~200 kyr, although volcanism in the area may have started

as early as ~340 ka (Gamble et al. 2003; Tost and Cronin 2015). Ruapehu lavas were grouped by Hackett (1985) into four formations that represent the main phases of edifice growth (Table 1): Te Herenga (200–150 ka), Wahianoa (160–115 ka), Mangawhero (50–15 ka), and Whakapapa (<15 ka). The absolute ages and durations of these formations were first constrained by Gamble et al. (2003), who primarily concentrated on the ~300 m-thick stack of Wahianoa Formation lavas exposed on the southeast flank of Ruapehu. Their data were recently combined with new $^{40}Ar/^{39}Ar$ ages by Conway et al. (2016) to provide a new geological map (summarised in Fig. 2) and to outline the revised edifice construction history summarised here. Sub-glacial to ice-marginal effusive eruption of medium-K basaltic-andesites and andesites constructed the northern portion of the exposed edifice between ~200 and 150 ka (Te Herenga), and a wide southeast planèze as well as parts of the northern, eastern and western flanks between ~160 and 80 ka (Wahianoa). No lava flows on the edifice have ages in the range of 80–50 ka, however, $^{40}Ar/^{39}Ar$ eruption ages measured for lava clasts within debris flow deposits indicate that there were some effusive eruptions during this period (Tost and Cronin 2015). The lack of dated lavas on the edifice for this period is likely to be the result of erosion and burial of lavas and/or syn-eruptive glacial conveyance of lava flows as debris to the ring-plain (Conway et al. 2016). In addition to bridging the apparent hiatus and extending the maximum age for volcanism at Ruapehu, other $^{40}Ar/^{39}Ar$ ages for clasts within distal debris flow deposits generally overlap with the timing of effusive volcanism recorded by in situ lavas of the Te Herenga and Wahianoa formations (Tost and Cronin 2015). From ~50–15 ka edifice growth occurred via effusive eruptions onto the glaciated flanks of the volcano, resulting in construction of ice-bounded planèzes and ridges (Mangawhero). Large-scale retreat of flank glaciers since ~15 ka has resulted in intra-valley lava flow emplacement at elevations below ~1500 m on the edifice. Conway et al. (2016) reported the first $^{40}Ar/^{39}Ar$ eruption ages for lava flows of the post-glacial Whakapapa

Formation in addition to 25 ages for lavas of the Mangawhero Formation, which together provide a comprehensive volcanic sequence to investigate time-composition relationships.

The greatest volume of lava flows on Ruapehu are plagioclase and pyroxene phyric andesites, however, basaltic-andesites and dacites have also been erupted at Ruapehu. Complex crystal and lithic cargoes are found throughout the eruptive products, which have been described in detail by Clark (1960), Cole (1978), Graham (1987), and Graham and Hackett (1987). The last authors defined six petrographically and geochemically distinct lava types with corresponding models of magma formation. These models accounted for the crust-like geochemical and isotopic composition of Ruapehu lavas by invoking partial melting and assimilation of mid-upper crustal greywacke-argillite basement during magma genesis (see also Graham 1987).

The overall development of the magma system beneath Ruapehu was later explored within stratigraphic contexts by Donoghue et al. (1995), Gamble et al. (1999, 2003), Waight et al. (1999, 2017) and Price et al. (2005). A model for the polybaric generation of derivative magmas by independent episodes of melting, mixing, assimilation and fractionation within an open magmatic system was generated from these studies (Price et al. 2012 for summary). This model allows for the non-systematic geochemical and isotopic variations observed over timescales ranging from short-lived explosive episodes and cycles (1–50 yr; Gamble et al. 1999; Auer et al. 2013; Kilgour et al. 2013) to successive lava flow emplacement phases (1–10 kyr; Waight et al. 1999; Gamble et al. 2003). Over the 200 kyr lifetime of the exposed Ruapehu edifice, however, a general progression towards more evolved compositions with time was proposed based on whole-rock geochemical variations using the available stratigraphic constraints (Graham and Hackett 1987; Price et al. 2012). In addition, the oldest exposed lavas (Te Herenga Formation) have distinct $^{143}Nd/^{144}Nd$–$^{87}Sr/^{86}Sr$ characteristics that set them apart from all subsequent lavas (Price et al. 2005). On this basis, Graham et al.

(1990) and Price et al. (2005, 2012) argued that Te Herenga Formation lavas were contaminated by Mesozoic oceanic basaltic rocks of the lower crust, whereas post-Te Herenga lavas assimilated partial melts of the basement greywacke-argillite sequence in the mid-upper crust.

Within the context of prior studies there are three key topics that we address here:

*1. Time-composition relationships.* Incomplete sampling of the edifice and a lack of chronological control hampered previous studies of the geochemical evolution of the Ruapehu magma system. Complex stratigraphic relationships as a result of lava-ice interaction (Conway et al. 2015) and sparse radiometric eruption age constraints previously precluded accurate definition of the relative and absolute ages for lava flows of the Mangawhero and Whakapapa formations that form much of the edifice. Combined with previous dating constraints by Gamble et al. (2003), new $^{40}Ar/^{39}Ar$ ages for Ruapehu lava flows have provided a high-resolution framework with which to interrogate geochemical data (Conway et al. 2016). By using geochemical data acquired for the same samples that have been directly dated and collected within chronostratigraphic constraints, we are able to assess the long-term evolution of magmatism at Ruapehu within closely defined spatial and temporal contexts, as has been done at other arc stratovolcanoes globally (e.g. Dungan et al. 2001; Hora et al. 2007; Jicha et al. 2012). Data from lava clasts in distal deposits and tephra in pyroclastic deposits have been integrated into this study where it is appropriate and possible to do so.

*2. Nature and origin of silicic melts.* Melt inclusion and matrix glass data compositions ranging from dacite to rhyolite have previously been described from Wahianoa Formation lavas, and Whakapapa Formation and historical lavas and pyroclasts (Donoghue et al. 1995; Gamble et al. 1999; Price et al. 2005; Kilgour et al. 2013; Pardo et al. 2014). In this

contribution we present the first glass geochemistry data for Te Herenga Formation eruptive products and a number of spatially distinct packages identified within the Mangawhero Formation. These new data contribute to models of magma genesis at Ruapehu.

*3. Felsic-mafic interactions.* In light of the abundance of rhyolitic melt compositions, is there evidence for mafic recharge in the generation of intermediate (andesite) magmas, as postulated from local (Donoghue et al. 1995; Nakagawa et al. 2002) and global (e.g. Kent et al. 2010) studies? Is this a common process involved in the generation of magnesian andesites and continental crust at volcanic arcs globally? Petrological and geochemical characteristics of a suite of high-MgO lavas are presented here to explore these concepts.

## SAMPLES AND METHODS

Samples used in this study were collected from lava flows on Ruapehu between 2012 and 2015. A full sample list is available in the Electronic Supplementary Material. Petrographic descriptions for Ruapehu lava flows have been presented by Cole (1978), Graham (1987), Graham and Hackett (1987), Graham et al. (1990), and Price et al. (2012). Brief descriptions are provided for the sample suite used here for completeness and because new portions of the edifice have been sampled. Ruapehu lava flows are in general moderately to highly porphyritic, with only rare examples with <10 % phenocrysts (term used herein to define macrocrystals with sizes >100 μm, but generally in the range of 0.3–1.0 mm). Plagioclase phenocrysts occur in all samples examined and most commonly have sieved cores with complexly zoned rims. Orthopyroxene, clinopyroxene and olivine phenocrysts are present throughout Ruapehu lavas in varying proportions. For the basaltic-andesite lavas of the Te Herenga and Whakapapa formations, clinopyroxene and orthopyroxene are equally abundant. Orthopyroxene is the major ferromagnesian phase in lavas of the Mangawhero

Formation. Amphibole occurs within Mangawhero dacite lavas studied here only as rare pseudomorphs that are replaced by symplectite assemblages of plagioclase, pyroxene, oxides and glass. The groundmasses of Ruapehu lavas typically consist of felted aggregates of microlites (i.e. <100 μm) of plagioclase and orthopyroxene with volumetrically minor but ubiquitous oxide phases and small patches of glass. Magnetite is the dominant oxide phase present throughout the groundmass of Ruapehu lavas, although rare ilmenite and spinel are also present. Patches of glass in microlite-free areas ~5–10 μm-wide are present only in samples acquired from the margins of rapidly chilled ice-bounded Mangawhero Formation flows and some glassy Whakapapa Formation flows.

Meta-sedimentary and meta-igneous xenoliths are present in all collected samples and are particularly common in lavas of the Mangawhero and Whakapapa formations. Meta-sedimentary types are typically fine-grained assemblages of plagioclase, orthopyroxene and magnetite, which are likely to be metamorphic equivalents (or refractory residua) of the greywacke crust beneath Ruapehu (Price et al. 2005). Some meta-sedimentary fragments also contain glass and biotite (e.g. Graham 1987). Meta-igneous granulite xenoliths are composed of plagioclase, orthopyroxene and ilmenite with minor clinopyroxene and olivine and display relict igneous or cumulate textures (Graham et al. 1990). A summary of the mineral chemistry data acquired for this study is presented in Table 2. Typical zoning features of the major mineral phases are displayed in Fig. 3. Further petrographic descriptions and full mineral chemistry data are provided in the Electronic Supplementary Material.

Fresh interiors of samples were acquired by using a diamond saw to cut away any remaining weathered surfaces. Samples were crushed and then milled using an agate or tungsten-carbide ring mill. Major element compositions for 238 whole-rock powder samples were determined using an ARL® 8420+ dual goniometer wavelength dispersive X-ray fluorescence (XRF) spectrometer at the Open University, United Kingdom. These XRF data

have been presented by Conway et al. (2016) for the purposes of defining chronostratigraphic eruptive packages, and are used here to investigate magmatic processes. A subset of 73 whole-rock powders used for major element analysis was selected for trace element analysis and prepared at Victoria University of Wellington (VUW). Trace element analysis was carried out by solution inductively coupled plasma mass spectrometry (ICP-MS), on a Thermo-Fisher Element2 sector-field ICP-MS equipped with an ESCI auto sampler at VUW using methods similar to those of Eggins et al. (1997). Major element compositions for minerals and glass in 15 lava samples were analysed by electron probe microanalysis (EPMA) using the JEOL JXA 8230 instrument at VUW. Thin sections were prepared from lava samples and carbon coated before analysis. Analysis of crystal phases was performed using a focussed electron beam (~1μm-wide) at a current of 12 nA and accelerating voltage of 15 kV. The beam was defocussed to a width of 5 μm during analysis of melt inclusion and groundmass glasses. Due to the commonly small sizes of melt inclusions and interstitial glass patches, a 5 μm spot was used (rather than 10 μm). Only melt inclusions in pyroxene hosts were analysed; plagioclase-hosted inclusions were not well-enough preserved for viable analysis. The current was reduced to 8 nA and counting times for Na were reduced to 15 seconds on the peak and 10 seconds for the background to minimise potential devolatilisation. Laser ablation ICP-MS analyses of interstitial glass and xenolith-hosted glass in dacite lava sample CC415 were carried out at VUW using a Resonetics RESOlutionS155-SE laser ablation system equipped with an ATL ArF Excimer laser (wavelength 193 μm), coupled to an Agilent 7500CS ICP-MS. Additional details of sample preparation and analysis can be found in the Electronic Supplementary Material and in Conway (2016).

## RESULTS AND DISCUSSION

This section presents new geochemical data that are placed within the context of a revised chronostratigraphy and existing data for Ruapehu, as well as regional and global studies of arc volcanism. As such, the results are presented together with a discussion of their relevance. New whole-rock major and trace element data are presented in Figs. 4–7, and existing whole-rock isotopic data from Price et al. (2012) are displayed in Fig. 8. New glass major element data are presented in Fig. 9 and compared to existing data from Ruapehu and Taupo volcanoes. The extended sample coverage and improved chronological sequencing of lava flows presented here makes it possible to advance more detailed models of the evolution of the Ruapehu magmatic system, and bring to light several key questions for global studies of arc volcanism, including:

- What are the scales of temporal and spatial variability in magma composition at continental composite volcanoes?
- Do long-term time-composition trends recorded in arc lavas reflect density filtering of magmas via edifice loading and sector collapse?
- What is the nature and origin of felsic (rhyolitic) melts that are captured in intermediate arc lavas?
- What effect does the progressive throughput of magma have on the crustal contamination of continental arc magmas?
- Are high-MgO andesites-dacites erupted at continental arc volcanoes the products of mantle melting processes, or magma mixing during transit through the crust?

## Compositional diversity of lavas in time and space at Ruapehu

Composite volcanoes are the surficial structures of polygenetic magmatism (Davidson and de Silva 2000). Volcanic maps and stratigraphies that are coupled with geochemical data can constrain the temporal and spatial scales of compositional heterogeneity within polygenetic magma systems that feed composite volcanoes (e.g. Frey et al. 2004; Hora et al. 2007). A summary of whole-rock compositions for Ruapehu volcano lava flows was presented by Price et al. (2012), however, the major and trace element variations between and within formations are re-evaluated here in light of the extended sampling coverage and improved geochronological control. Compositional heterogeneity within the Ruapehu magma plumbing system is investigated in this section, with a particular focus on the time window between 50 and 35 ka. Ruapehu lava whole-rock major and trace element bivariate diagrams are shown in Fig. 4, and a representative suite of analyses is presented in Table 3. A complete list of whole-rock major and trace element data is available in the Electronic Supplementary Material.

Te Herenga lavas exhibit a relatively narrow compositional range for all major and trace elements that is generally distinct from younger lavas, excepting some overlap with the Wahianoa Formation (Fig. 4). The most mafic lava flow sampled on Ruapehu volcano (CC348: 53.8 wt. % $SiO_2$, 6.75 wt. % MgO) was erupted at 186.2 ± 6.8 ka (2 s.d: Conway et al. 2016). A notable characteristic of Te Herenga lavas is their low $K_2O$ contents (Fig. 4) when compared to younger lavas, and incompatible trace element contents are essentially constant over their ~3 wt. % $SiO_2$ range (Fig. 4). Wahianoa Formation lavas are basaltic-andesites and andesites that exhibit slightly elevated $SiO_2$, and incompatible trace element contents when compared with Te Herenga Formation lavas (Fig. 4). Previously un-sampled lavas erupted from ~100–80 ka have major element compositions that generally match ~166–100 ka lavas of the Wahianoa Formation. Within the Wahianoa Formation, a distinct group of flows is identified by low-MgO and high-$Al_2O_3$ contents consistent with higher modal

abundances of plagioclase relative to pyroxene (Graham and Hackett 1987). Mangawhero Formation lavas are separated on the basis of the age data into early (50–35 ka), middle (35–26 ka) and late (26–15 ka) divisions in this contribution. Lavas of the ~50–35 ka suite are compositionally diverse, covering an 8.2 wt. % range in $SiO_2$ from basaltic-andesite to dacite. These flows show strong positive trends for incompatible trace element abundances and a distinct trend toward higher $K_2O$ and Rb contents when plotted against $SiO_2$ and compared to older and younger lavas (Fig. 4).

Despite the broadly linear relationship between $SiO_2$ and incompatible trace elements, lavas erupted between 50 and 35 ka can be further grouped into high- and low-MgO types. Reasons for the high-MgO compositions are discussed in a later section of the discussion, but their features are described here. The high-MgO trend is defined by lavas of the Mangaehuehu and Te Kohatu eruptive packages, and low-MgO andesites and dacites are grouped within the Ngahuinga and Mangaturuturu eruptive packages (Fig. 6). The Mananui dacite package, which consists of a spatially isolated flow on the northern flank of Ruapehu, has an intermediate MgO content. High-MgO andesites ($Mg\#_{60–69}$, where Mg# = 100Mg/[Mg + Fe]) and dacites ($Mg\#_{54–57}$) also exhibit relatively high Ni and low $Al_2O_3$ contents at equivalent $SiO_2$ values when compared to all other eruptive products from Ruapehu volcano (Figs. 4, 5). The timing of eruption for these high-MgO andesites, which span a 5.2 wt. % range in $SiO_2$ contents, is constrained by maximum and minimum ages of 45.4 ± 2.0 ka and 41.8 ± 1.8 ka (Conway et al. 2016). This is a noteworthy feature when considering that a comparable range of ~4.8 wt. % $SiO_2$ is defined by the ~300 m-thick sequence of Wahianoa Formation lavas exposed on southeast Ruapehu, which reflects a much longer period of volcanism from ~160–115 ka (Gamble et al. 2003). The trends defined by our new data imply that at least four geochemically distinctive magma types (high-MgO andesite; high-MgO dacite; mid-MgO dacite; low-MgO andesite and/or low-MgO dacite) were feeding spatially

dispersed lava flow packages with volumes of several $km^3$ to the south, west and north flanks of Ruapehu during the period from ~50–35 ka (Conway et al. 2016). This implies that magma batches with volumes substantially greater than those tapped by historical pyroclastic eruptions were able to remain compositionally isolated in the crust beneath Ruapehu (Gamble et al. 1999; Kilgour et al. 2013).

Lava flows emplaced on the western flank of Ruapehu volcano from ~35 to 26 ka exhibit $SiO_2$, $K_2O$ and trace element contents that are intermediate between the low-MgO andesites and dacites erupted at 50–35 ka. Late Mangawhero Formation lava flows erupted at ~26–15 ka are andesites and rare dacites. These flows define a less steep trend for $K_2O$ and incompatible trace elements (e.g. Rb, Zr) plotted against $SiO_2$ when compared to middle (~35–26 ka) and early (~50–35 ka) Mangawhero Formation lavas (Fig. 4). The major and trace element compositions of ~26–15 ka andesites generally overlap with younger flows of the Whakapapa Formation (Fig. 4), which are andesites and basaltic-andesites. Numerous eruptive packages within the Whakapapa Formation that were sourced from discrete vents and summit cones have been defined (Price et al. 2012; Conway et al. 2016). Taken together, Whakapapa Formation lavas define a $SiO_2$–$K_2O$ trend contiguous with ~26–15 ka Mangawhero Formation lavas (Fig. 4) and broadly overlap with post-glacial Plinian eruptive deposits (see Pardo et al. 2014; Conway et al. 2016).

Previously published bivariate major element plots showed a scatter of overlapping data for lavas of variable age (e.g. Fig. 10 in Price et al. 2012), however, the data presented here allows some key discriminations to be made between lavas of different ages. Pre-80 ka lavas do not show strong linear trends towards a unique end-member, but are tightly clustered around relatively low $SiO_2$ and $K_2O$ values (Fig. 4). Lavas that were erupted between ~50 and 26 ka and <26 ka define distinct $SiO_2$-$K_2O$ compositional trends: Te Kohatu package dacite (sample CC508; 37.6 ± 1.4 ka) forms a silicic end-member for 50–26 ka lava flows,

whereas Whakapapaiti package member dacite (sample CC513; 25.7 ± 3.8 ka) forms a silicic end-member for <26 ka lavas (Fig. 4). Although the preserved portion of the Whakapapaiti package dacite flows is volumetrically minor (see Fig. 10 in Conway et al. 2016), their eruptions delineate a change in the nature of magma differentiation after ~26 ka, which is addressed in the following sections.

## Potential role of density filtering of magma compositions

The eruptive products of composite volcanoes can cover the compositional spectrum from basalt to rhyolite. Although time-sequenced trends generally do not follow unique pathways of progressive evolution toward the silicic end of the spectrum (cf. Eichelberger et al. 2006), a common concept is that magma systems evolve toward producing more silicic eruptive products over long time periods (>100 kyr). This idea is founded on the association of non-evolved (mafic) eruptive products with stratigraphically old portions of volcanic edifices, and the eruption of more evolved lavas and, in some cases, the incidence of climactic explosive eruptions of silicic magma later in the history of composite volcanoes (e.g. Bacon and Lanphere 2006; Hora et al. 2007; Singer et al. 2008; Escobar-Wolf et al. 2010). Throughout the cycle of volcanism represented by the eruptive products, the corresponding development of evolved, relatively low-density intrusive complexes in the crust will impede higher-density, more mafic magmas from reaching the surface. This provides a feedback loop that may explain general trends toward more evolved magma compositions over time at some volcanoes (e.g. Bacon and Lanphere 2006). An alternative consideration is that the load imparted on a magma source region during the construction of a surficial volcanic edifice allows only the eruption of progressively more buoyant magmas as the load increases with cumulative growth of the volcano (Pinel and Jaupart 2000; Hora et al. 2007). With time the density of magmas will be lowered via crystal fractionation, enabling

389 them to overcome the critical density threshold imposed by loading of the edifice in order to
390 ascend and ultimately erupt (Pinel and Jaupart 2000). Conversely, unloading of an edifice via
391 deglaciation, erosion or sector collapse will reduce the confining pressure on magma
392 reservoirs and enable relatively dense magmas to ascend to the surface (Pinel and Jaupart
393 2005; Rawson et al. 2016). In this way, a composite volcano acts as a density filter for
394 eruptible magma compositions.

395 The time-sequenced variation of Ruapehu lava compositions provides a type study for
396 assessing whether density filtering affected erupted magma compositions, by using time-
397 composition plots (Fig. 6) and multi-element diagrams (Fig. 7) for illustration. For the latter,
398 whole-rock trace element contents have been normalised to values for average continental
399 crust (Rudnick and Gao 2003) in order to reflect the extent of crustal contamination. Existing
400 isotope data for Ruapehu lavas from Price et al. (2012) are also reviewed in this section (Fig.
401 8). Ruapehu lavas display a general increase in $SiO_2$, $K_2O$, and the incompatible trace
402 element ratio Rb/Zr from ~200 to 50 ka (i.e. lavas of the Te Herenga and Wahianoa
403 formations; Figs. 6, 7). A key difference between lavas of the Te Herenga and Wahianoa
404 formations is their Sr-Nd isotopic characteristics (Price et al. 2005, 2012). $^{87}Sr/^{86}Sr$ isotopic
405 compositions of Wahianoa Formation lavas overlap with the most radiogenic Te Herenga
406 Formation samples (~0.7050), however they have distinctly lower $^{143}Nd/^{144}Nd$ ratios (Fig. 8).
407 Eruptive compositions show extreme diversity between ~50 and 35 ka (Fig. 6). Lava
408 compositions range from basaltic-andesite to dacite during this period, and display a wide
409 range in incompatible trace element contents, which extend to the most continental crust-like
410 values for Ruapehu samples (Figs. 6, 7). Similarly, $^{87}Sr/^{86}Sr$ values are highest in dacites of
411 this period (Fig. 8). High Rb/Zr values for these dacites likely indicate addition to derivative
412 magmas of Rb from a potassic phase because Zr is unlikely to be fractionated by the mineral
413 assemblage. Lavas that have erupted since ~35 ka, however, define a trend opposite to that of

414 the earlier volcanic history: ~35–26 ka lava flows have a relatively narrow range of
415 compositions intermediate within the range defined by ~50–35 ka lavas, and younger flows
416 (<26 ka) exhibit progressively less silicic compositions with time (Fig. 6). Trends for $K_2O$
417 contents and Rb/Zr values display the same decreasing pattern as $SiO_2$ for post-26 ka lavas,
418 which also generally have lower $^{87}Sr/^{86}Sr$ values than 50–35 ka lavas (Fig. 6, 8).

419 In light of the hypothesised consequences of density filtering of magmas at growing
420 volcanic edifices, three observations within the geochemical evolution of Ruapehu lavas are
421 significant. First, the effusion of dacite following >150 kyr of edifice construction by
422 eruption of basaltic-andesites and andesites of the Te Herenga and Wahianoa formations.
423 Second, the reversion after ~18 kyr to more mafic lava compositions, which broadly overlaps
424 with the timing of deglaciation of the edifice, as well as Holocene sector collapse events
425 (Eaves et al. 2015; Conway et al. 2016). Third, more evolved samples generally have more
426 crust-like $^{87}Sr/^{86}Sr$ values.

427 With respect to the first observation, the 50–35 ka effusive episode occurred after the
428 construction of a composite edifice comprising the Te Herenga and Wahianoa formations that
429 contributed ≥110 $km^3$ of total eruptive products to the surface above the Ruapehu magmatic
430 system, during which time lava compositions generally became gradually more evolved (Fig.
431 6; Conway et al. 2016). Mangawhero Formation dacite lavas were erupted at ~40 ka, possibly
432 indicating that lower density magmas were able to overcome the critical density threshold
433 imposed by loading of the edifice in order to ascend and ultimately erupt. However, basaltic-
434 andesites were also erupted at the beginning of the 50–35 ka eruptive period with $SiO_2$
435 contents comparable to pre-80 ka lavas. The eruption of basaltic-andesite thus contradicts the
436 premise that a density filter biased the eruptible magma compositions at this time.

With respect to the second observation, there is a clear trend toward more mafic lavas erupted since ~26 ka, and Holocene lava flows are andesites to basaltic-andesites with $SiO_2$ contents ≤59 wt. % (excepting one late Holocene flow with 61.5 wt. % $SiO_2$). Although not exactly coincident with the onset of this compositional change, wholesale glacial retreat on Ruapehu from ~18 ka is inferred from regional paleoclimate records (Newnham et al. 2003), and corroborated by local moraine geochronology (Eaves 2015) and lava-ice interaction features (Conway et al. 2015). Furthermore, sector collapse of the northwest summit and upper flank at ~10.5 ka (Palmer and Neall 1989; Eaves et al. 2015) and the southeast summit at ~4.6 ka (Donoghue and Neall 2001) would have also contributed to a reduction of the vertical stress on the sub-volcanic system. The models of Pinel and Jaupart (2000, 2005) suggest that the reduction of the confining pressure on the magma reservoirs would have enabled relatively dense magmas to be erupted at Ruapehu since 18 ka. However, the loss of ice cover and the volume of material removed from the edifice during the sector collapse events (~1 $km^3$) is minor when compared to the total edifice volume (~150 $km^3$).

With respect to the third observation, the matching trends for the different elements suggest that some common process, or combination of processes, have controlled the compositional variation through time (Fig. 6). The general trend of more evolved lavas tending to have higher $^{87}Sr/^{86}Sr$ values (Fig. 8) indicates that assimilation of basement meta-sedimentary crust had a primary role, along with crystal fractionation, in the compositional development of post-Te Herenga Formation magmas (Graham and Hackett 1987; Price et al. 2012). Crust-normalised multielement diagrams also reflect this trend (Fig. 7). These relationships do not preclude the influence of a density filter, but are interpreted here to reflect a coupling between magma diversity and crustal assimilation, which relates more to the thermal condition of the lithosphere than the load imposed by construction (or destruction) of the volcanic edifice. Flux of melt from the mantle and tectonic activity are

462 also key controls of the timescales of magma generation, residence and eruption (e.g.
463 Schmidt and Grunder 2009). Data are not available to quantify the effect of these factors for
464 this study, however, because (1) past mantle-derived melt flux rates cannot be constrained by
465 surficial volcanic records, and (2) fault slip rate data are unable to resolve volcano-tectonic
466 processes on timescales of ~5–10 kyr in the Ruapehu Graben (Rowland et al. 2010; Gómez-
467 Vasconcelos et al. 2017).

468 In summary, it is considered unlikely that systematic trends within geochemical
469 evolution of Ruapehu lavas studied here were influenced primarily by near-surface processes.
470 Eruptions tapped magmas that had experienced variable degrees of differentiation in the crust
471 via crystal fractionation and crustal assimilation (Price et al. 2012). Thus, despite evidence
472 for compositional heterogeneity within eruptive sequences on annual to 10 kyr timescales
473 (e.g. Gamble et al. 1999, 2003), this study has defined a broadly coherent geochemical trend
474 for Ruapehu eruptive products over the ~200 kyr lifetime of the exposed edifice (Fig. 6). The
475 mechanisms of magma differentiation and the reasons for their varied influence through time
476 are now considered.

477

478 **Nature and origin of silicic melts in Ruapehu lavas**

479 Silicic glass compositions (often rhyolitic) for groundmass and melt inclusions in
480 phenocrysts of arc andesite-dacite volcanic rocks have been widely reported (e.g. Reubi and
481 Blundy 2009; Kent 2013; Lee and Bachmann 2014). Silicic melts can originate via one or
482 more of: assimilation of plutonic crystal cumulate roots (e.g. Reubi and Blundy 2008); partial
483 melting of subducted oceanic lithosphere and sediment (e.g. Tatsumi 2001); partial melting of
484 crustal rocks (e.g. Jackson et al. 2003); or fractionation of mantle-derived primary basaltic
485 magmas (e.g. Sisson et al. 2005). We focus on the latter two processes through the

compositions of glasses that represent trapped portions of melt from the Ruapehu magma system. Dacite to rhyolite compositions (~67–78 wt. % $SiO_2$) were measured for Ruapehu lava groundmass glass and pyroxene-hosted melt inclusions in this study (Fig. 9) and are compared to data from Ruapehu pyroclasts (Pardo et al. 2014) and Taupo volcano (Barker et al. 2015). Representative major element (Table 4) and trace element data (Table 5) are provided here, and full data are available in the Electronic Supplementary Material.

The silicic composition of Te Herenga Formation melt inclusions may not be a surprising result considering the ubiquity of such inclusion compositions in younger Ruapehu lavas (Price et al. 2005) and arc volcanic rocks globally (Reubi and Blundy, 2009). However, the low-$K_2O$ contents are notable, given that Te Herenga Formation lavas also have low-$K_2O$ whole-rock compositions (Figs. 4, 9). Melt inclusion and groundmass glasses within the high-MgO andesites and dacites of the early Mangawhero Formation have significantly higher $K_2O$ contents in comparison to Te Herenga samples (Fig. 9). Discordance between melt inclusion and groundmass glass compositions in the high-MgO andesite lavas may reflect late-stage magma mixing processes (see next section). $K_2O$ contents of up to 5–6 wt. % were measured for groundmass glasses, melt inclusions and xenolith-hosted glasses within dacite lavas. The pattern of the quenched melt network in the xenolith fragment within dacite sample CC415 that was analysed indicates that the melt was derived from partial melting of the xenolith (Fig. 3). This glass is also characterized by Rb contents of up to 270 ppm (Table 5). Melt inclusions in Whakapapa Formation lava flows exhibit a range of compositions that return to lower $K_2O$ contents (Fig. 9). The compositions presented here are broadly consistent with groundmass glass and melt inclusion data for historically erupted samples (Gamble et al. 1999; Kilgour et al. 2013) and previous analyses from Whakapapa Formation lavas (Price et al. 2012) and pyroclastic deposits (Pardo et al. 2014). Furthermore, the glass data are

intersected by the lower $SiO_2$–$K_2O$ trends defined by <26 ka lava whole-rock compositions when compared to earlier Mangawhero Formation lavas (Fig. 9).

Glass data for the different formations broadly align with their respective whole-rock trends that are age-constrained (Fig. 9), and therefore represent the products of different patterns of assimilation and fractional crystallization (AFC: DePaolo, 1981). The distinctive whole-rock $^{143}Nd/^{144}Nd$ isotopic compositions of Te Herenga lavas (Fig. 8; Price et al. 2005, 2012) have been inferred to reflect an early stage of the thermal evolution of the magma conduit system beneath Ruapehu attended by assimilation of mafic oceanic crust, which is considered to form the lower crust underlying the meta-sedimentary greywacke-argillite Torlesse Terrane sequence of middle to upper crustal rocks (Graham 1987; Price et al. 2012; Waight et al. 2017). Despite the limited amount of data, the distinct compositions of Te Herenga glasses support the idea that melts and magmas were generated by distinct petrogenetic processes during the ~200–150 ka time period when compared to subsequent magmatism. The role of assimilation of continental crust in the genesis of younger magmas has been previously documented, and high $^{87}Sr/^{86}Sr$ values for Mangawhero Formation dacites indicate that evolved magmas at Ruapehu experienced more mid-upper crustal contamination (Graham and Hackett 1987; Price et al. 2005, 2012; Fig. 8).

When compared to younger lavas, the high-$K_2O$ nature of glasses within the high-MgO lavas of the Mangawhero Formation is also considered here to represent AFC processing that involved relatively greater assimilation of mid-upper crust. This inference is supported by the observed Rb/Zr trends (Fig. 6): elevated values for evolved lavas would require addition of Rb from a crustal source given that Zr is unlikely to be fractionated by the phases observed in these samples. Metasedimentary crust assimilation is corroborated by radiogenic isotope data (Price et al. 2012; Waight et al. 2017), and evidence of this process was fortuitously captured by the analysis of a partially fused xenolith in sample CC415 (Fig.

3). We interpret that the entrained glass represents an *in situ* partial melt of a meta-sedimentary crustal rock with a significant contribution from melting of K-bearing minerals (such as biotite and K-feldspar) that are known to occur within the Torlesse Terrane basement rocks (Graham and Hackett 1987; Graham et al. 1990; Adams et al. 2009; Price et al. 2012). Published whole-rock $^{143}Nd/^{144}Nd$-$^{87}Sr/^{86}Sr$ systematics (Price et al. 2012; Waight et al. 2017) and trace element data indicate that Whakapapa Formation lavas were derived from magmas that were contaminated by continental crust, although to a lesser degree than the 50–35 ka Mangawhero Formation lavas (Figs. 7, 8).

Modelled chemical evolution pathways are presented in Fig. 10 in order to replicate these distinct conditions of magma differentiation. The La/Sm ratio is used to indicate the degree of evolution, and should be insensitive to compositional changes caused by crystal fractionation. Plotted against this ratio, Rb/Zr values should generally increase due to crystal fractionation because Rb is more incompatible than Zr. Significant differences in Rb/Zr versus La/Sm trends between lavas of different ages, however, will reflect variable addition of Rb from potassic phases in crustal rocks during assimilation. In general, post-26 ka lavas lie along a flatter trend than 50–35 ka lavas, which extend to higher Rb/Zr values at higher La/Sm values (Fig. 10). These broadly high and low trends for whole-rock Rb/Zr versus La/Sm variations are seen in lavas erupted from (1) 50–35 ka and (2) <26 ka, respectively. These trends can then be compared against modelled compositions for AFC evolution that involve: (1) a relatively high Rb/Zr contribution from a high-K crustal assimilant; and (2) a relatively low Rb/Zr contribution from a low-K crustal assimilant (Fig. 10). The compositions of the assimilants are constrained by *in situ* analyses of glass within meta-sedimentary xenoliths in lavas of the Mangawhero Formation (this study) and Whakapapa Formation (Price et al. 2005). Thus, assimilants were chosen because they have been observed and analysed within glasses in the host lavas of interest.

While there is overlap between lavas of the different periods, the modelled pathways aid the interpretation of two key features of the dataset. Firstly, the highest Rb/Zr values, which are observed for dacite lavas erupted from 50–35 ka, cannot be produced by AFC involving a low-K assimilant. Secondly, the low Rb/Zr values for post-26 ka lavas over a range of La/Sm values are best-approximated by magma differentiation via AFC involving a low-K assimilant. Post-26 ka magmas were likely generated during differentiation in a crustal melting scenario that was more advanced than at ~40 ka beneath Ruapehu due to the continued flux of magma through the lithosphere. In this regard, our modelling suggests that post-26 ka magmas interacted with crust that was relatively depleted in elements such as K and Rb when compared with those that fed the ~50–35 ka lavas. The difference is inferred to have been due to the progressive heating and partial melting of the crustal column, which is interpreted to have led to either or both of: (1) the exhaustion of fertile, K- and Rb-rich mineral phases that were consumed during earlier (50–35 ka) stages of upper crust assimilation; and (2) dilution effects reflecting the higher degrees of partial melting as magma flux continued through the crust beneath Ruapehu.

## A case for mafic recharge recorded in high-Mg andesite-dacites at Ruapehu

High-magnesian andesites (HMAs) are intermediate arc volcanic rocks (54–65 wt. % $SiO_2$) with high Mg# (≥50) and Cr and Ni concentrations (Kelemen et al. 2003a). At an extreme, the eruption of primitive HMAs with Mg# ~70, although rare, is of particular importance because such magmas may be produced by partial melting of hydrous mantle peridotite (e.g. Grove et al. 2002, 2005; Wood and Turner 2009) and therefore play a fundamental role in the genesis of arc magmas and continental crust (Kelemen et al. 2003b). Other models for the petrogenesis of HMAs invoke equilibration of slab-derived melts with

584 ultramafic mantle wedge material (e.g. Kay 1978; Shimoda et al. 1998; Tatsumi 2001;
585 Yogodzinski et al. 2001) and felsic-mafic magma mixing combined with entrainment of
586 ultramafic crystal material within arc lithosphere (e.g. Kawabata and Shuto 2005; Streck et al.
587 2007). HMAs have been studied at Mt Shasta in the Cascade arc (Anderson 1973; Grove et
588 al. 2002; Streck et al. 2007) and the Setouchi volcanic belt in southwest Japan (Shimoda et al.
589 1998; Kawabata and Shuto 2005). New Zealand examples have erupted at White Island
590 ($Mg\#_{70}$: Heyworth et al. 2007), Pukeonake ($Mg\#_{50}$: Graham and Hackett 1987; Beier et al.
591 2017) and Hauhungatahi ($Mg\#_{70}$: Cameron et al. 2010). Ruapehu high-MgO lavas were
592 described by Graham and Hackett (1987), but corresponding models of their generation
593 lacked the chronostratigraphic context (Conway et al. 2016) and microanalytical data
594 discussed here.

595 Andesite and dacite lavas of the Mangaehuehu and Te Kohatu eruptive packages,
596 respectively, are HMAs with whole-rock Mg# for the lavas ranging from 60–69 (andesites)
597 and 54–57 (dacites). Mangaehuehu package andesites exhibit high MgO contents over a ~5
598 wt. % $SiO_2$ range, and Te Kohatu package dacites (~65 wt. % $SiO_2$) have MgO contents that
599 are notably higher than other Ruapehu dacite lavas (Fig. 4). The Ruapehu HMAs also show
600 high Ni contents (up to 148 ppm) compared to other Ruapehu lavas at equivalent $SiO_2$
601 contents (Fig. 4). A petrographic feature that distinguishes these HMA lavas from lower-
602 MgO flows at Ruapehu is their high proportions of resorbed orthopyroxene that are mantled
603 by euhedral rims with high Mg# values (~85–90: Fig. 3). The HMAs also contain
604 metasedimentary xenoliths, indicating that their source magmas interacted with and
605 assimilated crustal rocks. The petrographic and geochemical characteristics indicate that
606 derivative magmas underwent substantial fractionation and assimilation processes in the
607 lithosphere and do not represent near-primary melting products of the mantle wedge.

608 Comparisons are made in Fig. 5 between the composition of Ruapehu lavas and the
609 relatively primitive Waimarino and Kakuki basalts from the central Taupo Volcanic Zone to
610 the north (Gamble et al. 1993), as well as the Pukeonake and Ohakune andesites, which were
611 erupted from peripheral vents located ~20 km from the summit of Ruapehu (Figs. 1, 2, 5).
612 Eruptive activity at the Ruapehu peripheral vents pre-dates the Oruanui tephra (25.4 ka;
613 Vandergoes et al. 2013) as indicated by stratigraphic relations (Hackett, 1985; Froggatt and
614 Lowe, 1990), and is likely to have occurred within the period ~40–30 ka,
615 penecontemperoneous with the high-Mg lavas from Ruapehu (50–35 ka). The high-MgO
616 suite of Ruapehu lavas trends toward the composition of Waimarino basalt, and is
617 approximately intercepted by the composition of Pukeonake and Ohakune andesites (Fig. 6).
618 Low-MgO lavas erupted from 50–35 ka define a trajectory from Mangaturuturu package
619 dacite toward Kakuki basalt, which is broadly intercepted by all post-35 ka and pre-80 ka
620 lavas from the Ruapehu edifice.

621 Pukeonake lavas have been described as hybrid andesites and their compositions can
622 be modelled by mixing between dacite and Waimarino basalt (Graham and Hackett 1987;
623 Beier et al. 2017). Ruapehu HMAs are similarly interpreted here to have been produced via
624 mixing between a deeper-sourced mafic magma and a mid- to upper crustal-level felsic
625 magma. Clusters of orthopyroxene preserved in the HMAs display high-MgO rims only on
626 the outermost exposed margins of the crystal clots (Fig. 3), indicating that the mafic magma
627 encountered a crystal-rich magma and interacted with crystal margins that were in contact
628 with the mafic magma during disaggregation of the crystal assemblage (cf. Nakagawa et al.
629 2002; Fig. 3). Subsequent crystal growth occurred within the hotter magma and accounts for
630 the higher MgO rims around the resorbed cores. Evidence for interaction between recharging
631 higher temperature magmas and stagnant, more felsic magmas has also been reported in the
632 ~11 ka Pourahu (Donoghue et al. 1995) and 1995-1996 Ruapehu eruptives (Nakagawa et al.

2002). Whole-rock Mg# values of ~60 for such samples are not as high as for Ruapehu HMAs with equivalent $SiO_2$ contents reported in this study, which may reflect a greater contribution from the mafic end-member within the Mangawhero Formation HMAs. The comparable crystal zonation features are interpreted to reflect a similar process for older lavas and younger examples, however, and has been documented elsewhere. In particular, similar pyroxene zoning features and magma mixing processes have been described for HMAs from Mt Shasta (Streck et al. 2007, figure 2) and the Setouchi volcanic belt (Kawabata and Shuto 2005, figure 7).

Constraining the nature of primitive magmas in the southern end of the Taupo Volcanic Zone is difficult because even relatively primitive basaltic-andesites have generally undergone textural and chemical modification in the crust (Waight et al. 2017). The reverse-zoned crystal cargo of HMAs provides only a cryptic record of mafic magma intrusion into the crust beneath Ruapehu. Comparison to regional primitive lavas, however, yields insight into the spatial distribution of such an end-member with respect to regional volcanism. The shared petrogenetic origin of hybrid andesites at Ruapehu and within its periphery (Pukeonake and Ohakune) may indicate the presence of a common mafic end-member within the Tongariro Volcanic Centre as well as the broader Taupo Volcanic Zone.

## IMPLICATIONS

We have presented new whole-rock, mineral and glass compositions for edifice-forming lavas within a high-resolution eruption chronology for Ruapehu volcano. Together with existing isotopic data and petrogenetic models, these data further clarify the evolution of the Ruapehu magma system and provide a case study for continental arc volcanism. The long-term compositional variability of lava flows during the ~200 kyr lifetime of the exposed

Ruapehu edifice offers snapshots into the crustal dynamics of an evolving arc magmatic system. Major implications are as follows.

- The broadly coincident effusion of at least 4 compositionally distinct lava flow packages during the ~50–35 ka time window at Ruapehu indicates the existence of a compositionally heterogeneous central magma system. Reconstructed vent locations for each lava package indicates that discrete magma batches were spatially and compositionally distinctive despite (in some cases) being vented within 2 km of each other. These results indicate that relatively large-scale heterogeneities can exist within the magma systems feeding composite volcanoes, as well as the more commonly cited small-scale heterogeneities that are tapped by explosive eruptions of relatively low-volume and ephemeral magma batches at Ruapehu (e.g. Gamble et al. 1999; Auer et al. 2013; Kilgour et al. 2013).

- The systematic geochemical evolution of Ruapehu lavas is unlikely to have been influenced primarily by density filtering of eruptible magma compositions due to loading and unloading of the edifice. Instead, eruptions tapped magmas that had undergone variable degrees of differentiation in the crust via crystal fractionation and crustal assimilation. The effect of crustal assimilation on magma compositions was greatest for the period from ~50–35 ka, due to the progressive advection of heat through the lithosphere leading to partial melting and assimilation of mid- to upper crustal meta-sedimentary country rocks. Post-26 ka magmas are interpreted to have assimilated less enriched melts due to the prior consumption of fertile phases in the crustal column and/or higher degrees of partial melting of continental crust associated with ongoing magma and heat flux through the magma system. A similar ~200 kyr time-composition trend has been shown for Volcán Parinacota (Hora et al. 2007).

- The compositional similarity between the groundmass glass of a dacite lava and a xenolith-hosted partial melt within that lava (sample CC415) confirms the importance of crustal assimilation in the geochemical characteristics of eruptive products at continental arc volcanoes. However, to better constrain the processes involved, further work is required to characterise the mineralogy and isotopic composition of the crustal lithologies beneath Ruapehu volcano, as well as the composition of the primary magmas.

- High-MgO andesites and dacites that were erupted between ~50 and 35 ka at Ruapehu were produced via interaction between felsic and mafic magmas. Clusters of pyroxene were entrained from the more felsic magma reservoirs by the influx of hotter, more mafic magma, and were then resorbed and overgrown by Mg-rich rims. Ruapehu high-Mg andesites and dacites represent magmas resulting from middle to upper crustal-level assimilation and mixing processes rather than being primary magmas derived directly by mantle melting.

## ACKNOWLEDGEMENTS

This work was part-funded by Department of Conservation contract DOCDM-593774. CEC was supported by Victoria University of Wellington DVC Research Grant 13311 and a postdoctoral research fellowship from the Japan Society for the Promotion of Science (JSPS P16788). Field and laboratory support was provided by James Brigham-Watson, Jason Marshall and Kirsten Henden. The late John Watson of the Open University, UK, carried out the XRF analyses. Assistance with other analyses was provided by Ian Schipper (EPMA), Simon Barker, Monica Handler (ICPMS), and Dan Sinclair (LA-ICPMS). We extend our

704 thanks to Maurizio Petrelli for the editorial handling, and to two anonymous reviewers.
705 Michelle Coombs provided helpful comments on an earlier version of this manuscript.

706

## 707 REFERENCES CITED

708 Adams, C.J., Mortimer, N., Campbell, H.J., and Griffin, W.L. (2009) Age and isotopic
709 characteristics of metasedimentary rocks from the Torlesse Supergroup and Waipapa
710 Group in the central North Island, New Zealand. New Zealand Journal of Geology and
711 Geophysics, 52, 149-170.
712 Anderson, A.T. (1973) The before-eruption water content of some high-alumina magmas.
713 Bulletin Volcanologique, 37, 243-267.
714 Auer, A., White, J.D.L., Nakagawa, M., and Rosenburg, M.D. (2013). Petrological record
715 from young Ruapehu eruptions in the 4.5 ka Kiwikiwi Formation, Whangaehu Gorge,
716 New Zealand. New Zealand Journal of Geology and Geophysics, 56, 121-133.
717 Bacon, C.R., and Lanphere, M.A. (2006) Eruptive history and geochronology of Mount
718 Mazama and the Crater Lake region, Oregon. Geological Society of America Bulletin,
719 118, 1331-1359.
720 Barker, S.J., Wilson, C.J.N., Allan, A.S.R., and Schipper, C.I. (2015) Fine-scale temporal
721 recovery, reconstruction and evolution of a post-supereruption magmatic system.
722 Contributions to Mineralogy and Petrology, 170, 5.
723 Beier, C., Haase, K.M., Brandl, P.A., and Krumm, S.H. (2017) Primitive andesites from the
724 Taupo Volcanic Zone formed by magma mixing. Contributions to Mineralogy and
725 Petrology, 172, 33.

726 Cameron, E., Gamble, J., Price, R, Smith, I., McIntosh, W., and Gardner, M. (2010) The
727 petrology, geochronology and geochemistry of Hauhungatahi volcano, S.W. Taupo
728 Volcanic Zone. Journal of Volcanology and Geothermal Research, 190, 179-191.
729 Clark, R.H. (1960) Appendix II: Petrology of the volcanic rocks of Tongariro Subdivision.
730 In: Gregg, D.R. (Ed.) The geology of Tongariro Subdivision: New Zealand Geological
731 Survey Bulletin, 40, 107–123.
732 Clynne, M.A. (1999) A complex magma mixing origin for rocks erupted in 1915, Lassen
733 Peak, California. Journal of Petrology, 40, 105-132.
734 Cole, J.W. (1978) Andesites of the Tongariro Volcanic Centre, North Island, New Zealand.
735 Journal of Volcanology and Geothermal Research, 3, 121-153.
736 Cole, J.W. (1990) Structural control and origin of volcanism in the Taupo Volcanic Zone,
737 New Zealand. Bulletin of Volcanology, 52, 445-459.
738 Conway, C.E. (2016) Studies on the glaciovolcanic and magmatic evolution of Ruapehu
739 volcano, New Zealand. PhD thesis, Victoria University of Wellington, New Zealand,
740 259 pp. http://hdl.handle.net/10063/5152.
741 Conway, C.E., Townsend, D.B., Leonard, G.S., Wilson, C.J.N., Calvert, A.T., and Gamble,
742 J.A. (2015) Lava-ice interaction on a large composite volcano: a case study from
743 Ruapehu, New Zealand. Bulletin of Volcanology, 77, 21.
744 Conway, C.E., Leonard, G.S., Townsend, D.B., Calvert, A.T., Wilson, C.J.N., Gamble, J.A.,
745 and Eaves, S.R. (2016) A high-resolution $^{40}Ar/^{39}Ar$ lava chronology and edifice
746 construction history for Ruapehu volcano, New Zealand. Journal of Volcanology and
747 Geothermal Research, 327, 152-179.
748 Coombs, M.L., Eichelberger, J.C., and Rutherford, M.J. (2000) Magma storage and mixing
749 conditions for the 1953-1974 eruptions of Southwest Trident volcano, Katmai National
750 Park, Alaska. Contributions to Mineralogy and Petrology, 140, 99-118.

751 Coombs, M.L., Sisson, T.W., Bleick, H.A., Henton, S.M., Nye, C.J., Payne, A.L., Cameron,
752 C.E., Larsen, J.F., Wallace, K.L., and Bull, K.F. (2013) Andesites of the 2009 eruption
753 of Redoubt Volcano, Alaska. Journal of Volcanology and Geothermal Research, 259,
754 349-372.
755 Davidson, J., and de Silva, S. (2000) Composite volcanoes. In: Sigurdsson, H., Houghton,
756 B.F., Rymer, H., Stix, J., and McNutt, S. (Eds.) Encyclopedia of Volcanoes, Academic
757 Press, p. 663-681.
758 Davidson, J.P., Morgan, D.J., Charlier, B.L.A., Harlou, R., and Hora, J.M. (2007)
759 Microsampling and isotopic analysis of igneous rocks: implications for the study of
760 magmatic systems. Annual Review of Earth and Planetary Sciences, 35, 273-311.
761 DePaolo, D.J. (1981) Trace element and isotopic effects of combined wallrock assimilation
762 and fractional crystallization. Earth and Planetary Science Letters, 53, 189-202.
763 Donoghue, S.L., and Neall, V.E. (2001) Late Quaternary constructional history of the
764 southeastern Ruapehu ring plain, New Zealand. New Zealand Journal of Geology and
765 Geophysics, 44, 439-466.
766 Donoghue, S.L., Gamble, J.A., Palmer, A.S., and Stewart, R.B. (1995) Magma mingling in an
767 andesite pyroclastic flow of the Pourahu Member, Ruapehu volcano, New Zealand.
768 Journal of Volcanology and Geothermal Research, 68, 177-191.
769 Dungan, M.A., and Davidson, J. (2004) Partial assimilative recycling of the mafic plutonic
770 roots of arc volcanoes: an example from the Chilean Andes. Geology, 32, 773-776.
771 Dungan, M.A., Wulff, A., and Thompson, R. (2001) Eruptive stratigraphy of the Tatara-San
772 Pedro Complex, 36°S, Southern Volcanic Zone, Chilean Andes: reconstruction method
773 and implications for magma evolution at long-lived arc volcanic centres. Journal of
774 Petrology, 42, 555-626.

775 Eaves, S.R. (2015) The glacial history of Tongariro and Ruapehu volcanoes, New Zealand.
776 PhD thesis, Victoria University of Wellington, 253 pp.
777 Eaves, S.R., Winckler, G., Schaefer, J.M., Vandergoes, M.J., Alloway, B.V., Mackintosh,
778 A.M., Townsend, D.B., Ryan, M.T., and Li, X (2015) A test of the cosmogenic $^{3}$He
779 production rate in the south-west Pacific (39°S). Journal of Quaternary Science, 30, 79-
780 87.
781 Eggins, S.M., Woodhead, J.D., Kinsley, L.P.J., Mortimer, G.E., Sylvester, P., McCulloch,
782 M.T., Hergt, J.M., and Handler, M.R. (1997) A simple method for the precise
783 determination of ≥40 trace elements in geological samples by ICPMS using enriched
784 isotope internal standardisation. Chemical Geology, 134, 311-326.
785 Eichelberger, J.C. (1975) Origin of andesite and dacite: evidence for mixing at Glass
786 Mountain in California and other circum-Pacific volcanoes. Geological Society of
787 America Bulletin, 86, 1381-1391.
788 Eichelberger, J.C., Izbekov, P.E., and Browne, B.L. (2006) Bulk chemical trends at arc
789 volcanoes are not liquid lines of descent. Lithos, 87, 135-154.
790 Escobar-Wolf, R.P., Diehl, J.F., Singer, B.S., and Rose, W.I. (2010) $^{40}$Ar/$^{39}$Ar and
791 paleomagnetic constraints on the evolution of Volcan de Santa Maria, Guatemala.
792 Geological Society of America Bulletin, 122, 757-771.
793 Frey, H.M., Lange, R.A., Hall, C.M., and Delgado-Granados, H. (2004) Magma eruption
794 rates constrained by $^{40}$Ar/$^{39}$Ar chronology and GIS for the Ceboruco-San Pedro
795 volcanic field, western Mexico. Geological Society of America Bulletin, 116, 259-276.
796 Froggatt, P.C., and Lowe, D.J. (1990) A review of late Quaternary silicic and some other
797 tephra formations from New Zealand: their stratigraphy, nomenclature, distribution,
798 volume, and age. New Zealand Journal of Geology and Geophysics, 33, 89-109.

799 Gamble, J.A., Smith, I.E.M., McCulloch, M.T., Graham, I.J., and Kokelaar, B.P. (1993) The
800 geochemistry and petrogenesis of basalts from the Taupo Volcanic Zone and the
801 Kermadec Island Arc, S.W., Pacific. Journal of Volcanology and Geothermal Research,
802 54, 265-290.
803 Gamble, J.A., Wood, C.P., Price, R.C., Smith, I.E.M., Stewart, R.B., and Waight, T. (1999) A
804 fifty year perspective of magmatic evolution on Ruapehu Volcano, New Zealand:
805 verification of open system behaviour in an arc volcano. Earth and Planetary Science
806 Letters, 170, 301-314.
807 Gamble, J.A., Price, R.C., Smith, I.E.M., McIntosh, W.C., and Dunbar, N.W. (2003)
808 $^{40}Ar/^{39}Ar$ geochronology of magmatic activity, magma flux and hazards at Ruapehu
809 Volcano, Taupo Volcanic Zone, New Zealand. Journal of Volcanology and Geothermal
810 Research, 120, 271-287.
811 Gómez-Vasconcelos, M.G., Villamor, P., Cronin, S., Procter, J., Palmer, A., Townsend, D.,
812 and Leonard, G. (2017) Crustal extension in the Tongariro Graben, New Zealand:
813 Insights into volcano-tectonic interactions and active defoemtion in a young continental
814 rift. Geological Society of America Bulletin, 129, 1085-1099.
815 Graham, I.J. (1987) Petrography and origin of metasedimentary xenoliths in lavas from
816 Tongariro Volcanic Centre. New Zealand Journal of Geology and Geophysics, 30, 139-
817 157.
818 Graham, I.J., and Hackett, W.R. (1987) Petrology of calc-alkaline lavas from Ruapehu and
819 related vents, Taupo Volcanic Zone, New Zealand. Journal of Petrology, 28, 531-567.
820 Graham, I.J., Blattner, P., and McCulloch, M.T. (1990) Meta-igneous xenoliths from Mount
821 Ruapehu, New Zealand: fragments of altered oceanic crust? Contributions to
822 Mineralogy and Petrology, 105, 650-661.

823 Grove, T.L., Parman, S.W., Bowring, S.A., Price, R.C., and Baker, M.B. (2002) The role of
824 an $H_2O$-rich fluid component in the generation of primitive basaltic andesites and
825 andesites from the Mt. Shasta region, N California. Contributions to Mineralogy and
826 Petrology, 142, 375-396.
827 Grove, T.L., Baker, M.B., Price, R.C., Parman, S.W., Elkins-Tanton, L.T., Chatterjee, N., and
828 Müntener, O. (2005) Magnesian andesite and dacite lavas from Mt. Shasta, northern
829 California: products of fractional crystallization of $H_2O$-rich mantle melts.
830 Contributions to Mineralogy and Petrology, 148, 542-565.
831 Hackett, W.R. (1985) Geology and petrology of Ruapehu volcano and related vents. PhD
832 thesis, Victoria University of Wellington, New Zealand, 467 pp.
833 Hackett, W.R., Houghton, B.F. (1989) A facies model for a Quaternary andesitic composite
834 volcano, Ruapehu, New Zealand. Bulletin of Volcanology, 51, 51-68.
835 Heyworth, Z., Turner, S., Schaefer, B., Wood, B., George, R., Berlo, K., Cunningham, H.,
836 Price, R., Cook, C., and Gamble, J. (2007) $^{238}U$–$^{230}Th$–$^{226}Ra$–$^{210}Pb$ constraints on the
837 genesis of high-Mg andesites at White Island, New Zealand. Chemical Geology, 243,
838 105-121.
839 Hildreth, W., and Fierstein, J. (2012) Eruptive history of Mount Katmai, Alaska. Geosphere,
840 8, 1527-1567.
841 Hildreth, W., Fierstein, J., and Lanphere, M.A. (2003) Eruptive history and geochronology of
842 the Mount Baker volcanic field, Washington. Geological Society of America Bulletin,
843 115, 729-764.
844 Hobden, B.J., Houghton, B.F., Davidson, J.P., and Weaver, S.D. (1999) Small and short-lived
845 magma batches at composite volcanoes: time windows at Tongariro volcano, New
846 Zealand. Journal of the Geological Society, London, 156, 865-868.

847 Hora, J.M., Singer, B.S., and Worner, G. (2007) Volcano evolution and eruptive flux on the
848 thick crust of the Andean Central Volcanic Zone: $^{40}Ar/^{39}Ar$ constraints from Volcan
849 Parinacota, Chile. Geological Society of America Bulletin, 119, 343-362.
850 Jackson, M.D., Cheadle, M.J., and Atherton, M.P. (2003) Quantitative modelling of granitic
851 melt generation and segregation in the continental crust. Journal of Geophysical
852 Research, 108, 2332.
853 Kawabata, H., and Shuto, K. (2005) Magma mixing recorded in intermediate rocks associated
854 with high-Mg andesites from the Setouchi volcanic belt, Japan: implications for
855 Archean TTG formation. Journal of Volcanology and Geothermal Research, 140, 241-
856 271.
857 Kay, R.W. (1978) Aleutian magnesian andesites: melts from subducted Pacific Ocean crust.
858 Journal of Volcanology and Geothermal Research, 4, 117-132.
859 Kelemen, P.B., Hanghoj, K., and Green, A.R. (2003a) One view of the geochemistry of
860 subduction-related magmatic arcs, with an emphasis on primitive andesites and the
861 lower crust. In: Rudnick, R.L. (Ed.) The Crust, in: Holland, H.D., and Turekian, K.K.
862 (Eds.) Treatise on Geochemistry, Elsevier, Oxford, UK, 3, 593-659.
863 Kelemen, P.B., Yogodzinski, G.M., and Scholl, D.W. (2003b) Along-strike variation in the
864 Aleutian island arc: genesis of high-Mg# andesite and implications for continental
865 crust. In: Eiler, J. (Ed.) Inside the Subduction Factory, American Geophysical Union
866 Geophysical Monographs, 138, 223-276.
867 Kent, A.J.R. (2013) Preferential eruption of andesitic magmas: implications for volcanic
868 magma fluxes at convergent margins. In: Gomez-Tuena, A., Straub, S., M., and Zellmer
869 G.F. (Eds.) Orogenic Andesites and Crustal Growth, Geological Society of London,
870 Special Publications, 385, 257-280.

871 Kent, A.J.R., Darr, C., Koleszar, A.M., Salisbury, M.J., and Cooper, K.M. (2010) Preferential
872 eruption of andesitic magma through recharge filtering. Nature Geoscience, 3, 631-636.
873 Kilgour, G., Blundy, J., Cashman, K., and Mader, H.M. (2013) Small volume andesite
874 magmas and melt-mush interactions at Ruapehu, New Zealand: evidence from melt
875 inclusions. Contributions to Mineralogy and Petrology, 166, 371-392.
876 Koleszar, A.M., Kent, A.J.R., Wallace, P.J., and Scott, W.E. (2012) Controls on long-term
877 low explosivity at arc volcanoes: insights from Mount Hood, Oregon. Journal of
878 Volcanology and Geothermal Research, 219-220, 1-14.
879 Lee, C.-T.A., and Bachmann, O. (2014) How important is the role of crystal fractionation in
880 making intermediate magmas? Insights from Zr and P systematics. Earth and Planetary
881 Science Letters, 393, 266-274.
882 Nakagawa, M., Wada, K., and Wood, C.P. (2002) Mixed magmas, mush chambers and
883 eruption triggers: evidence from zoned clinopyroxene phenocrysts in andesitic scoria
884 from the 1995 eruptions of Ruapehu volcano, New Zealand. Journal of Petrology, 43,
885 2279-2303.
886 Newnham, R.M., Eden, D.N., Lowe, D.J., and Hendy, C.H. (2003) Rerewhakaaitu Tephra, a
887 land-sea marker for the Last Termination in New Zealand, with implications for global
888 climate change. Quaternary Science Reviews, 22, 289-308.
889 Palmer, B.A., and Neall, V.E. (1989) The Murimotu Formation–9500 year old deposits of a
890 debris avalanche and associated lahars, Mount Ruapehu, North Island, New Zealand.
891 New Zealand Journal of Geology and Geophysics, 32, 477-486.
892 Pardo, N., Cronin, S.J., Wright, H.M.N., Schipper, C.I., Smith, I., and Stewart, B. (2014)
893 Pyroclast textural variation as an indicator of eruption column steadiness in andesitic
894 Plinian eruptions at Mt. Ruapehu. Bulletin of Volcanology, 76:822.

895 Petrelli, M., Poli, G., Perugini, D., and Peccerillo, A. (2005) PetroGraph: A new software to
896 visualize, model, and present geochemical data in igneous petrology. Geochemistry,
897 Geophysics, Geosystems, 6, Q07011.
898 Pinel, V., and Jaupart, C. (2000) The effect of edifice load on magma ascent beneath a
899 volcano. Philosophical Transactions of the Royal Society of London, A358, 1515-1532.
900 Pinel, V., and Jaupart, C. (2005) Some consequences of volcanic edifice destruction for
901 eruption conditions. Journal of Volcanology and Geothermal Research, 145, 68-80.
902 Price, R.C., Gamble, J.A., Smith, I.E.M., Stewart, R.B., Eggins, S., and Wright, I.C. (2005)
903 An integrated model for the temporal evolution of andesites and rhyolites and crustal
904 development in New Zealand's North Island. Journal of Volcanology and Geothermal
905 Research, 140, 1-24.
906 Price, R.C., Gamble, J.A., Smith, I.E.M., Maas, R., Waight, T., Stewart, R.B., and
907 Woodhead, J. (2012) The anatomy of an andesite volcano: a time-stratigraphic study of
908 andesite petrogenesis and crustal evolution at Ruapehu Volcano, New Zealand. Journal
909 of Petrology, 53, 2139-2189.
910 Price, R.C., Mortimer, N., Smith, I.E.M., Maas, R. (2015) Whole-rock geochemical reference
911 data for Torlesse and Waipapa terranes, North Island, New Zealand. New Zealand
912 Journal of Geology and Geophysics, 58, 213–228.
913 Rawson, H., Pyle, D.M., Mather, T.A., Smith, V.C., Fontijn, K., Lachowycz, S.M., and
914 Naranjo, J.A. (2016) The magmatic and eruptive response of arc volcanoes to
915 deglaciation: insights from southern Chile. Geology, 44, 251-254.
916 Reubi, O., and Blundy, J. (2008) Assimilation of plutonic roots, formation of high-K 'exotic'
917 melt inclusions and genesis of andesitic magmas at Volcàn de Colima, Mexico. Journal
918 of Petrology, 49, 2221-2243.

Reubi, O., and Blundy, J. (2009) A dearth of intermediate melts at subduction zone volcanoes and the petrogenesis of arc andesites. Nature, 461, 1269-1273.

Rowland, J.V., Wilson, C.J.N., and Gravley, D.M. (2010) Spatial and temporal variations in magma-assisted rifting, Taupo Volcanic Zone, New Zealand. Journal of Volcanology and Geothermal Research, 190, 89-108.

Rudnick, R.L., and Gao, S. (2003) Composition of the continental crust. In: Rudnick, R.L. (Ed.) The Crust, in: Holland, H.D., and Turekian, K.K. (Eds.) Treatise on Geochemistry, Elsevier, Oxford, 3, 1-64.

Schmidt, M.E., and Grunder A.L. (2009) The evolution of North Sister: a volcano shaped by extension and ice in the central Oregon Cascade Arc. Geological Society of America Bulletin, 121, 643-662.

Shimoda, G., Tatsumi, Y., Hohda, S., Ishizaka, K., and Jahn, B.M. (1998) Setouchi high-Mg andesites revisited: geochemical evidence for melting of subducting sediments. Earth and Planetary Science Letters, 160, 479-492.

Singer, B.S., Jicha, B.R., Harper, M.A., Naranjo, J.A., Lara, L.E., and Moreno-Roa, H. (2008) Eruptive history, geochronology, and magmatic evolution of the Puyehue-Cordón-Caulle volcanic complex, Chile. Geological Society of America Bulletin, 120, 599-618.

Sisson, T.W., Ratajeski, K., Hankins, W.B., and Glazner, A.F. (2005) Voluminous granitic magmas from common basaltic sources. Contributions to Mineralogy and Petrology, 148, 635-661.

Sisson, T.W., Salters, V.J.M., and Larson, P.B. (2013) Petrogenesis of Mount Rainier andesite: magma flux and geologic controls on the contrasting differentiation styles at stratovolcanoes of the southern Washington Cascades. Geological Society of America Bulletin, 126, 122-144.

944 Streck, M.J., Leeman, W.P., and Chesley, J. (2007) High-magnesian andesite from Mount
945 Shasta: a product of magma mixing and contamination, not a primitive mantle melt.
946 Geology, 35, 351-354.
947 Tatsumi, Y. (2001) Geochemical modelling of partial melting of subducting sediments and
948 subsequent melt-mantle interaction: generation of high-Mg andesites in the Setouchi
949 volcanic belt, southwest Japan. Geology, 29, 323-326.
950 Tost, M., and Cronin, S.J. (2015) Linking distal volcaniclastic sedimentation and stratigraphy
951 with the development of Ruapehu volcano, New Zealand. Bulletin of Volcanology, 77,
952 94.
953 Tost, M., Price, R.C., Cronin, S.J., and Smith, I.E.M. (2016) New insights into the evolution
954 of the magmatic system of a composite andesite volcano revealed by clasts from distal
955 mass-flow deposits: Ruapehu volcano, New Zealand. Bulletin of Volcanology, 78, 38.
956 Vandergoes, M.J., Hogg, A.G., Lowe, D.J., Newnham, R.M., Denton, G.H., Southon, J.,
957 Barrell, D.J.A., Wilson, C.J.N., McGlone, M.S., Allan, A.S.R., Almond, P.C., Petchey,
958 F., Dabell, K., Dieffenbacher-Krall, A.C., and Blaauw, M. (2013) A revised age for the
959 Kawakawa/Oruanui tephra, a key marker for the Last Glacial Maximum in New
960 Zealand. Quaternary Science Reviews, 74, 195-201.
961 Waight, T.E., Price, R.C., Smith, I.E.M., Stewart, R.B., and Gamble, J.A. (1999) Stratigraphy
962 and geochemistry of the Turoa region, with implications for andesite petrogenesis at
963 Mt. Ruapehu, Taupo Volcanic Zone, New Zealand. New Zealand Journal of Geology
964 and Geophysics, 42, 513-532.
965 Waight, T.E., Troll, V.R., Gamble, J.A., Price, R.C., and Chadwick, J.P. (2017) Hf isotope
966 evidence for variable slab input and crustal addition in basalts and andesites of the
967 Taupo Volcanic Zone, New Zealand. Lithos 284-285, 222-236.

968 Wilson, C.J.N., Houghton, B.F., McWilliams, M.O., Lanphere, M.A., Weaver, S.D., Briggs,
969 R.M. (1995) Volcanic and structural evolution of Taupo Volcanic Zone, New Zealand -
970 a review. Journal of Volcanology and Geothermal Research, 68, 1–28.

971 Wood, B.J., and Turner, S.P. (2009) Origin of primitive high-Mg andesites: constraints from
972 natural examples and experiments., Earth and Planetary Science Letters, 283, 59-66.

973 Yogodzinski, G.M., Lees, J.M., Churikova, T.G., Dorendorf, F., Wörner, G., and Volynets,
974 O.N. (2001) Geochemical evidence for the melting of subducting oceanic lithosphere at
975 plate edges. Nature, 409, 500-504.

976

977

978

979

980

981

982

983

984

985

986

987

988

989 Table 1. Summary of chronostratigraphic formations and eruptive packages for edifice-
990 forming lava flows at Ruapehu volcano (modified from Conway et al. 2016).

| Formation | Eruptive Package |
|---|---|
| Whakapapa (<15 ka) | Crater Lake<br>Iwikau<br>Saddle Cone<br>Tureiti<br>Paretetaitonga<br>Rangataua<br>Turoa |
| Mangawhero late (26-15 ka) | Makotuku<br>Waitonga<br>Te Piripiri<br>Horonuku<br>Whakapapaiti |
| Mangawhero middle (35-26 ka) | Manganuiotaeo |
| Mangawhero early (50-35 ka) | Mananui<br>Te Kohatu<br>Mangaturuturu<br>Mangaehuehu<br>Ngahuinga |
| Wahianoa (160-80 ka) | Undifferentiated |
| Te Herenga (200-150 ka) | Undifferentiated |

991

992

993

994

995

996

997

998

999

1000

1001 Table 2. Summary of EPMA data for major mineral phases in Ruapehu lavas.

| Sample Information | | | | Whole-rock | | Phenocryst compositional range (rim) | | | |
|---|---|---|---|---|---|---|---|---|---|
| **Number** | **Fmtn** | **Package** | **Age (ka)** | **$SiO_2$ (wt.%)** | **Mg#** | **Opx (Mg #)** | **Cpx (Mg #)** | **Plg (An %)** | **Ol (Mg #)** |
| CC281 | WH | SC | 10 | 56.0 | 56 | 62-77 (68-80) | 65-85 (59-81) | 52-81 (67-80) | 73-75 |
| CC260 | WH | TR | 12 | 57.4 | 52 | 63-68 (68-78) | 67-81 (71-75) | 50-90 (56-73) | na |
| CC335 | WH | PT | 15 | 58.5 | 51 | 61-77 (65-70) | 69-84 (71-73) | 54-89 (58-88) | 70-72 |
| CC193 | WH | RT | 15 | 59.3 | 47 | 61-69 (65-71) | 70-74 (71-73) | 50-87 (53-79) | na |
| CC415 | MA | TK | 38 | 64.2 | 55 | 59-86 (58-90) | 72-77 (67-86) | 38-64 (45-62) | 72-75 |
| CC479 | MA | TK | 38 | 64.9 | 54 | 59-86 (58-73) | 70-87 (67-88) | 40-70 (42-63) | na |
| CC313 | MA | TK | 42 | 64.4 | 57 | 49-85 (54-74) | 67-83 (66-88) | 38-81 (33-65) | na |
| CC069 | MA | ME | 42 | 59.3 | 65 | 68-90 (68-85) | 72-88 (72-85) | 48-82 (40-70) | 82-84 |
| CC077 | MA | ME | 42 | 60.1 | 65 | 65-84 (69-90) | 68-89 (72-87) | 50-83 (52-60) | na |
| CC154 | MA | ME | 42 | 60.9 | 64 | 69-82 (61-89) | 70-85 (74-80) | 42-76 (46-61) | 78-80 |
| CC089 | MA | ME | 43 | 58.7 | 66 | 70-78 (77-89) | 72-78 (69-87) | 53-68 (51-70) | 78-80 |
| CC125 | MA | ME | 44 | 56.8 | 69 | 69-90 (67-89) | 72-86 (80-84) | 48-60 (55-63) | na |
| CC308 | TH | - | 170 | 57.0 | 54 | 67-70 (60-61) | 71-83 (70-71) | 56-82 (40-67) | na |
| CC326 | TH | - | 170 | 55.2 | 53 | 65-72 (54-60) | 70-74 (72-74) | 61-82 (78-79) | 69-70 |
| CC348 | TH | - | 187 | 53.8 | 59 | 67-76 (66-77) | 63-86 (73-84) | 68-86 (49-70) | 70-85 |

1002

1003 Notes. Formation abbreviations are WH (Whakapapa), MA (Mangawhero), and TH (Te
1004 Herenga). Package abbreviations are SC (Saddle Cone), TR (Turoa), PT (Paretetaitonga), RT
1005 (Rangataua), TK (Te Kohatu) and ME (Mangaehuehu). $SiO_2$ (in weight %) and values of
1006 Mg# [100Mg/(Mg + Fe)] are shown for whole-rock lava. Ranges of Mg# values determined
1007 by EPMA are shown for orthopyroxene (Opx), clinopyroxene (Cpx) and olivine (Olv)
1008 phenocrysts and their rims (in parentheses). Anorthite % shown for analyses of plagioclase
1009 (Plg) phenocrysts and rims (in parentheses). NA indicates not analysed. Full data are in the
1010 Electronic Supplementary Material.

1011

1012

1013

1014

1015

1016

This is a preprint, the final version is subject to change, of the American Mineralogist (MSA)
Cite as Authors (Year) Title. American Mineralogist, in press.
DOI: https://doi.org/10.2138/am-2018-6199

1017 Table 3. Whole-rock major and trace element data for representative Ruapehu lavas.

| Sample | GL1983 | GL1030 | CC335 | CC130 | CC226 | CC364 | CC408 | CC143 | CC513 | CC462 | CC547 |
|---|---|---|---|---|---|---|---|---|---|---|---|
| Package | CL | IW | PT | TR | MK | TP | MK | WT | WH | MG | MG |
| Age (ka) | 0±2 | 6±2 | 15±3 | 15±2 | 18±2 | 21±6 | 21±3 | 23±2 | 26±4 | 31±2 | 31±5 |
| $SiO_2$ | 61.45 | 57.30 | 58.51 | 60.08 | 61.37 | 58.29 | 60.87 | 62.26 | 65.61 | 60.73 | 62.46 |
| $TiO_2$ | 0.72 | 0.68 | 0.73 | 0.70 | 0.89 | 0.70 | 0.78 | 0.67 | 0.62 | 0.86 | 0.81 |
| $Al2O_3$ | 15.71 | 16.71 | 17.09 | 15.91 | 17.25 | 16.08 | 17.28 | 16.20 | 14.88 | 16.87 | 17.00 |
| $Fe_2O_3$ | 6.41 | 7.57 | 7.51 | 6.59 | 6.03 | 7.57 | 6.42 | 5.84 | 5.02 | 6.49 | 5.74 |
| MnO | 0.10 | 0.12 | 0.12 | 0.10 | 0.09 | 0.12 | 0.10 | 0.10 | 0.08 | 0.10 | 0.09 |
| MgO | 3.94 | 5.20 | 3.96 | 4.95 | 2.52 | 5.22 | 2.64 | 3.58 | 3.43 | 3.23 | 2.44 |
| CaO | 6.03 | 7.67 | 7.16 | 6.51 | 5.91 | 7.34 | 6.02 | 5.59 | 4.50 | 6.10 | 5.15 |
| $Na_2O$ | 3.25 | 3.21 | 3.22 | 3.25 | 3.68 | 3.00 | 3.75 | 3.56 | 3.69 | 3.41 | 3.56 |
| $K_2O$ | 2.23 | 1.39 | 1.57 | 1.76 | 2.07 | 1.54 | 1.97 | 2.03 | 2.06 | 2.03 | 2.56 |
| $P_2O_5$ | 0.16 | 0.14 | 0.14 | 0.14 | 0.18 | 0.14 | 0.17 | 0.17 | 0.11 | 0.19 | 0.19 |
| LOI | -0.13 | 0.12 | -0.15 | 0.01 | -0.17 | -0.07 | -0.10 | 0.05 | 0.36 | -0.16 | 0.24 |
| Total | 99.19 | 100.41 | 99.63 | 99.44 | 99.95 | 98.92 | 99.08 | 99.89 | 100.25 | 100.00 | 99.49 |
| | | | | | | | | | | | |
| Li | 22.1 | 19.9 | 15.9 | 20.7 | 22.2 | 13.6 | 25.7 | 26.7 | 27.0 | 21.6 | 31.3 |
| Sc | 19.7 | 25.2 | 24.4 | 22.1 | 17.2 | 27.2 | 17.9 | 17.7 | 15.4 | 19.6 | 15.8 |
| V | 159 | 194 | 199 | 161 | 195 | 205 | 172 | 128 | 120 | 172 | 144 |
| Ni | 34.7 | 65.2 | 18.2 | 66.8 | 13.4 | 41.0 | 7.7 | 52.4 | 49.9 | 19.0 | 14.5 |
| Cu | 21.6 | 34.6 | 26.3 | 33.3 | 14.6 | 50.8 | 32.7 | 29.9 | 18.4 | 28.9 | 23.5 |
| Zn | 61.5 | 66.3 | 77.5 | 59.3 | 58.8 | 68.4 | 66.7 | 59.9 | 73.1 | 68.2 | 60.6 |
| Ga | 17.0 | 18.3 | 19.2 | 17.6 | 18.8 | 16.9 | 19.4 | 18.1 | 17.4 | 18.5 | 18.6 |
| Rb | 86.3 | 46.8 | 59.2 | 62.7 | 78.4 | 57.4 | 69.0 | 75.5 | 84.7 | 72.6 | 110.2 |
| Sr | 251 | 299 | 257 | 264 | 304 | 225 | 305 | 266 | 229 | 305 | 258 |
| Y | 19.7 | 17.9 | 21.2 | 16.8 | 20.8 | 19.8 | 19.6 | 20.0 | 13.7 | 21.9 | 23.2 |
| Zr | 151 | 96 | 119 | 123 | 153 | 113 | 136 | 133 | 149 | 153 | 172 |
| Nb | 5.86 | 4.03 | 4.81 | 5.31 | 6.17 | 4.54 | 5.13 | 6.23 | 6.77 | 6.53 | 7.18 |
| Cs | 3.68 | 1.79 | 2.02 | 2.70 | 2.62 | 2.07 | 2.13 | 2.80 | 3.45 | 2.66 | 2.96 |
| Ba | 408 | 337 | 338 | 355 | 452 | 311 | 417 | 409 | 410 | 425 | 454 |
| La | 15.0 | 10.0 | 13.7 | 12.5 | 16.0 | 12.2 | 14.9 | 15.6 | 8.7 | 17.9 | 19.9 |
| Ce | 32.9 | 22.2 | 29.4 | 26.7 | 35.1 | 26.7 | 32.9 | 34.7 | 17.7 | 38.7 | 41.6 |
| Pr | 4.03 | 2.77 | 3.64 | 3.29 | 4.35 | 3.35 | 3.95 | 4.26 | 2.21 | 4.74 | 5.27 |
| Nd | 15.8 | 11.9 | 14.7 | 13.1 | 17.1 | 13.6 | 16.1 | 17.1 | 9.1 | 19.0 | 21.0 |
| Sm | 3.52 | 2.97 | 3.38 | 3.02 | 3.77 | 3.12 | 3.58 | 3.69 | 2.21 | 4.22 | 4.48 |
| Eu | 0.90 | 0.87 | 0.92 | 0.86 | 1.01 | 0.85 | 0.97 | 0.90 | 0.71 | 1.08 | 1.05 |
| Gd | 3.78 | 2.94 | 3.62 | 3.05 | 3.82 | 3.51 | 3.72 | 3.71 | 2.31 | 4.33 | 4.68 |
| Tb | 0.55 | 0.49 | 0.57 | 0.47 | 0.57 | 0.53 | 0.54 | 0.58 | 0.37 | 0.63 | 0.66 |
| Dy | 3.39 | 2.99 | 3.59 | 2.97 | 3.46 | 3.38 | 3.44 | 3.42 | 2.34 | 3.82 | 4.07 |
| Ho | 0.69 | 0.61 | 0.74 | 0.59 | 0.73 | 0.71 | 0.70 | 0.68 | 0.50 | 0.77 | 0.81 |
| Er | 2.04 | 1.77 | 2.14 | 1.76 | 2.10 | 2.07 | 1.99 | 2.02 | 1.48 | 2.23 | 2.38 |
| Tm | 0.30 | 0.27 | 0.32 | 0.27 | 0.30 | 0.30 | 0.30 | 0.30 | 0.22 | 0.32 | 0.33 |
| Yb | 2.02 | 1.78 | 2.13 | 1.75 | 2.05 | 2.03 | 1.94 | 1.86 | 1.47 | 2.07 | 2.26 |
| Lu | 0.29 | 0.27 | 0.33 | 0.26 | 0.30 | 0.30 | 0.29 | 0.27 | 0.22 | 0.31 | 0.33 |
| Hf | 4.06 | 2.71 | 3.26 | 3.44 | 4.12 | 3.12 | 3.63 | 3.62 | 4.01 | 4.02 | 4.49 |
| Pb | 12.8 | 7.15 | 9.27 | 10.5 | 10.2 | 7.49 | 9.47 | 17.1 | 12.0 | 10.5 | 9.83 |
| Th | 8.12 | 4.34 | 5.67 | 5.97 | 7.32 | 5.35 | 6.46 | 6.43 | 6.42 | 7.24 | 8.85 |
| U | 2.21 | 1.22 | 1.43 | 1.60 | 1.85 | 1.42 | 1.63 | 1.73 | 1.91 | 1.76 | 2.41 |

1018

1019

1020 Table 3 (continued).

| Sample | CC508 | CC570 | CC125 | CC216 | CC424 | CC470 | CC562 | CC209 | CC213 | CC326 | CC348 |
|---|---|---|---|---|---|---|---|---|---|---|---|
| Package | TK | MN | ME | ME | NG | MT | WA | WA | WA | TH | TH |
| Age (ka) | 38±1 | 40±2 | 43±1 | 43±1 | 40±3 | 41±2 | 88±6 | 121±4 | 121±3 | 170±8 | 186±7 |
| $SiO_2$ | 65.03 | 63.57 | 56.80 | 60.19 | 59.34 | 63.49 | 57.55 | 58.36 | 58.40 | 55.24 | 53.79 |
| $TiO_2$ | 0.71 | 0.85 | 0.70 | 0.77 | 0.76 | 0.83 | 0.62 | 0.68 | 0.70 | 0.65 | 0.67 |
| $Al2O_3$ | 15.27 | 15.84 | 14.25 | 15.00 | 16.81 | 16.74 | 16.51 | 19.70 | 17.25 | 17.21 | 16.62 |
| $Fe_2O_3$ | 4.74 | 5.51 | 7.44 | 6.55 | 6.52 | 5.27 | 7.38 | 6.06 | 7.40 | 9.16 | 9.20 |
| MnO | 0.07 | 0.08 | 0.12 | 0.10 | 0.10 | 0.08 | 0.12 | 0.09 | 0.12 | 0.15 | 0.15 |
| MgO | 2.86 | 2.80 | 8.61 | 5.53 | 4.22 | 2.21 | 5.60 | 2.34 | 4.36 | 5.30 | 6.75 |
| CaO | 4.45 | 4.87 | 7.67 | 6.36 | 6.81 | 4.87 | 7.82 | 7.49 | 6.89 | 8.42 | 9.17 |
| $Na_2O$ | 3.42 | 3.50 | 2.85 | 3.28 | 3.48 | 3.64 | 3.37 | 3.92 | 3.31 | 3.12 | 2.82 |
| $K_2O$ | 3.27 | 2.78 | 1.41 | 2.05 | 1.80 | 2.68 | 0.93 | 1.22 | 1.44 | 0.66 | 0.71 |
| $P_2O_5$ | 0.18 | 0.20 | 0.14 | 0.18 | 0.16 | 0.20 | 0.11 | 0.13 | 0.13 | 0.09 | 0.11 |
| LOI | 0.10 | -0.02 | -0.10 | -0.02 | -0.11 | 0.20 | -0.09 | 0.06 | 0.11 | 0.01 | -0.25 |
| Total | 100.28 | 99.44 | 99.89 | 100.20 | 99.07 | 99.62 | 99.54 | 100.16 | 99.90 | 99.27 | 99.39 |
| | | | | | | | | | | | |
| Li | 36.7 | 31.0 | 19.5 | 23.6 | 20.0 | 24.8 | 14.9 | 13.6 | 21.7 | 10.2 | 8.34 |
| Sc | 14.3 | 15.8 | 27.1 | 21.6 | 19.9 | 16.0 | 27.0 | 16.8 | 23.9 | 32.0 | 34.5 |
| V | 121 | 143 | 191 | 164 | 170 | 146 | 196 | 175 | 188 | 233 | 249 |
| Ni | 30.4 | 36.7 | 175.9 | 123.3 | 49.2 | 12.1 | 54.9 | 15.4 | 30.1 | 28.6 | 54.7 |
| Cu | 27.9 | 39.1 | 39.2 | 88.5 | 37.4 | 12.3 | 47.6 | 93.8 | 43.1 | 74.0 | 38.3 |
| Zn | 30.2 | 68.0 | 61.8 | 59.2 | 60.8 | 66.5 | 70.1 | 64.6 | 81.0 | 87.1 | 81.4 |
| Ga | 17.8 | 18.6 | 15.5 | 17.3 | 18.4 | 19.0 | 17.8 | 20.9 | 18.8 | 17.9 | 17.5 |
| Rb | 144 | 111 | 52.8 | 79.7 | 61.8 | 105 | 25.4 | 36.2 | 44.9 | 16.6 | 17.5 |
| Sr | 203 | 232 | 227 | 241 | 252 | 243 | 289 | 327 | 250 | 211 | 226 |
| Y | 23.2 | 23.5 | 17.5 | 21.8 | 18.5 | 21.3 | 14.6 | 19.1 | 19.2 | 18.9 | 18.7 |
| Zr | 215 | 199 | 114 | 150 | 130 | 186 | 69.3 | 92.8 | 101 | 59.4 | 58.5 |
| Nb | 9.00 | 8.36 | 4.16 | 6.26 | 4.58 | 7.22 | 3.00 | 3.79 | 4.46 | 1.83 | 1.89 |
| Cs | 5.15 | 3.83 | 2.32 | 2.38 | 2.00 | 3.30 | 0.61 | 1.07 | 1.56 | 0.42 | 0.37 |
| Ba | 552 | 509 | 302 | 404 | 345 | 495 | 236 | 316 | 332 | 184 | 222 |
| La | 20.9 | 20.2 | 10.6 | 16.7 | 12.8 | 16.6 | 6.23 | 11.0 | 11.4 | 5.44 | 6.01 |
| Ce | 45.3 | 44.0 | 23.5 | 35.7 | 28.4 | 36.5 | 14.5 | 22.8 | 25.7 | 11.3 | 13.5 |
| Pr | 5.43 | 5.31 | 2.90 | 4.40 | 3.50 | 4.53 | 1.93 | 3.00 | 3.29 | 1.69 | 1.94 |
| Nd | 21.0 | 21.5 | 12.0 | 18.1 | 14.6 | 18.0 | 8.43 | 12.7 | 13.5 | 7.67 | 8.97 |
| Sm | 4.53 | 4.56 | 2.95 | 3.92 | 3.29 | 4.01 | 2.10 | 3.05 | 3.22 | 2.17 | 2.38 |
| Eu | 0.91 | 1.01 | 0.82 | 0.93 | 0.87 | 1.03 | 0.71 | 0.92 | 0.87 | 0.74 | 0.81 |
| Gd | 4.59 | 4.60 | 3.08 | 4.09 | 3.40 | 4.18 | 2.29 | 3.12 | 3.27 | 2.55 | 2.81 |
| Tb | 0.64 | 0.66 | 0.48 | 0.62 | 0.50 | 0.59 | 0.39 | 0.49 | 0.52 | 0.45 | 0.46 |
| Dy | 3.88 | 4.11 | 2.92 | 3.75 | 3.22 | 3.67 | 2.58 | 3.11 | 3.29 | 3.09 | 3.08 |
| Ho | 0.80 | 0.82 | 0.60 | 0.75 | 0.65 | 0.74 | 0.53 | 0.65 | 0.68 | 0.68 | 0.67 |
| Er | 2.23 | 2.35 | 1.78 | 2.18 | 1.83 | 2.16 | 1.51 | 1.90 | 1.94 | 1.97 | 1.98 |
| Tm | 0.32 | 0.34 | 0.26 | 0.33 | 0.27 | 0.32 | 0.23 | 0.28 | 0.30 | 0.30 | 0.29 |
| Yb | 2.15 | 2.23 | 1.67 | 2.08 | 1.78 | 2.15 | 1.52 | 1.80 | 1.95 | 1.99 | 1.92 |
| Lu | 0.32 | 0.33 | 0.25 | 0.31 | 0.26 | 0.32 | 0.24 | 0.28 | 0.29 | 0.31 | 0.30 |
| Hf | 5.40 | 5.30 | 2.97 | 4.17 | 3.41 | 4.92 | 1.99 | 2.57 | 2.85 | 1.73 | 1.73 |
| Pb | 17.1 | 17.5 | 7.69 | 12.4 | 12.4 | 12.8 | 4.99 | 7.37 | 27.3 | 6.00 | 3.63 |
| Th | 12.1 | 10.0 | 4.91 | 7.08 | 5.82 | 9.82 | 2.36 | 3.39 | 4.15 | 1.40 | 1.63 |
| U | 3.58 | 2.70 | 1.29 | 2.02 | 1.49 | 2.59 | 0.65 | 0.93 | 1.10 | 0.44 | 0.43 |

1021

1022 Notes. Major oxide values are in weight % and are normalised to anhydrous totals (100 wt.

1023 %) with LOI (loss on ignition) and original analytical totals displayed. Trace elements

contents are in ppm. Package and Formation abbreviations are: Crater Lake (CL); Paretetaitonga (PT); Tureiti (TR); Makotuku (MK); Waitonga (WT); Whakapapaiti (WH); Manganuioteao (MG); Te Kohatu (TK); Mananui (MN); Mangaehuehu (ME); Ngahuinga (NG); Mangaturuturu (MT); Wahianoa Formation (WA); Te Herenga Formation (TH). Full data are in the Electronic Supplementary Material. Ages are $^{40}Ar/^{39}Ar$ weighted mean plateau ages from Conway et al. (2016).

1045 Table 4. Summary of melt inclusion and xenolith and groundmass glass compositions.

| Group | Value | $SiO_2$ | $TiO_2$ | $Al_2O_3$ | FeO | CaO | $Na_2O$ | $K_2O$ | Total |
|---|---|---|---|---|---|---|---|---|---|
| **WH** | avg | 74.0 | 0.5 | 14.9 | 1.1 | 1.9 | 3.6 | 3.8 | 99.6 |
| **mi** | max | 77.0 | 1.4 | 19.0 | 2.2 | 3.6 | 4.5 | 5.6 | 100.5 |
| **n= 45** | min | 70.3 | 0.2 | 13.0 | 0.5 | 1.0 | 0.8 | 1.8 | 98.4 |
| | 2sd | 3.7 | 0.4 | 2.6 | 0.8 | 1.4 | 1.3 | 2.2 | 1.3 |
| **WH** | avg | 73.8 | 1.2 | 12.2 | 3.1 | 1.0 | 3.4 | 5.0 | 99.7 |
| **gms** | max | 75.1 | 1.4 | 12.5 | 3.8 | 1.1 | 4.1 | 5.2 | 100.3 |
| **n=16** | min | 73.3 | 1.0 | 11.7 | 2.5 | 0.7 | 3.2 | 4.1 | 98.1 |
| | 2sd | 1.0 | 0.2 | 0.5 | 0.6 | 0.2 | 0.4 | 0.5 | 1.4 |
| **TK** | avg | 73.0 | 0.7 | 13.7 | 2.1 | 1.3 | 3.3 | 5.4 | 99.9 |
| **mi** | max | 75.6 | 1.2 | 16.2 | 3.3 | 2.8 | 4.2 | 6.2 | 100.8 |
| **n=67** | min | 70.0 | 0.2 | 12.1 | 1.0 | 0.7 | 1.0 | 4.0 | 98.5 |
| | 2sd | 3.0 | 0.5 | 2.5 | 0.9 | 1.0 | 0.9 | 1.1 | 1.1 |
| **TK** | avg | 73.8 | 1.0 | 12.7 | 2.3 | 1.0 | 3.0 | 5.8 | 98.0 |
| **i/x** | max | 75.2 | 1.3 | 15.5 | 2.8 | 1.4 | 3.7 | 6.3 | 99.0 |
| **n=17** | min | 70.5 | 0.7 | 12.1 | 1.7 | 0.9 | 2.7 | 5.5 | 97.1 |
| | 2sd | 2.7 | 0.4 | 1.9 | 0.6 | 0.2 | 0.4 | 0.4 | 1.1 |
| **TK** | avg | 74.4 | 0.8 | 12.6 | 2.2 | 1.2 | 3.0 | 5.5 | 101.0 |
| **gms** | max | 75.4 | 0.8 | 15.1 | 2.7 | 2.3 | 3.8 | 5.9 | 101.8 |
| **n=13** | min | 71.7 | 0.6 | 12.0 | 1.7 | 0.8 | 2.7 | 4.4 | 100.3 |
| | 2sd | 2.1 | 0.1 | 1.7 | 0.4 | 0.9 | 0.6 | 0.8 | 0.8 |
| **ME** | avg | 72.8 | 0.6 | 15.1 | 1.3 | 1.8 | 4.0 | 4.2 | 100.0 |
| **mi** | max | 67.6 | 0.1 | 13.0 | 0.4 | 0.6 | 3.0 | 3.2 | 99.0 |
| **n=30** | min | 76.6 | 1.9 | 17.5 | 3.0 | 3.6 | 7.2 | 5.6 | 100.6 |
| | 2sd | 4.9 | 1.0 | 2.0 | 1.4 | 1.6 | 1.4 | 1.1 | 0.8 |
| **ME** | avg | 69.4 | 1.7 | 13.0 | 5.1 | 2.5 | 4.5 | 3.0 | 99.9 |
| **gms** | max | 70.1 | 1.8 | 13.8 | 5.8 | 2.9 | 5.0 | 3.4 | 100.4 |
| **n=13** | min | 69.0 | 1.6 | 12.3 | 4.3 | 2.4 | 4.1 | 2.6 | 99.3 |
| | 2sd | 0.7 | 0.1 | 0.8 | 0.8 | 0.3 | 0.5 | 0.5 | 0.5 |
| **TH** | avg | 72.7 | 0.5 | 15.9 | 1.5 | 2.4 | 4.3 | 2.4 | 100.4 |
| **mi** | max | 78.7 | 1.1 | 17.8 | 2.1 | 3.4 | 5.9 | 3.5 | 101.8 |
| **n=24** | min | 69.7 | 0.1 | 12.9 | 0.6 | 1.3 | 1.6 | 1.7 | 98.1 |
| | 2sd | 5.6 | 0.8 | 3.0 | 0.8 | 1.1 | 1.6 | 0.8 | 2.0 |

1046

1047 Notes. Major oxide values are in weight % and are normalised to anhydrous totals (100 wt.
1048 %). Table is divided into groups of analyses from melt inclusions (mi), groundmass glass
1049 (gms), and interstitial and xenolith glass (i/x) from within different formations or packages:
1050 Whakapapa Formation (WH), Te Kohatu package, Mangawhero Formation (TK),
1051 Mangaehuehu package, Mangawhero Formation (ME), Te Herenga Formation (TH). From
1052 multiple analyses of glass within each group, values are displayed for average (avg),
1053 maximum (max), minimum (min) contents for each element, as well as 2 s.d. compositional
1054 variability. Full data are in the Electronic Supplementary Material.

1055 Table 5. LA-ICPMS trace element data for xenolith and interstitial glass.

| Sample | X1-1 | X2-1 | X2-2 | IG40-1 | IG12 (n=7) |
|---|---|---|---|---|---|
| **Sc** | 11.6 | 11.1 | 9.9 | 10.6 | 12 ± 2 |
| **V** | 64.6 | 52.6 | 32.7 | 70.3 | 57 ± 28 |
| **Zn** | 40.7 | 33.2 | 46.9 | 50.9 | 50 ± 7 |
| **Rb** | 255 | 274 | 273 | 272 | 271 ± 12 |
| **Sr** | 56.3 | 57.4 | 49.5 | 90.5 | 55 ± 6 |
| **Y** | 35.5 | 36.1 | 31.9 | 31.4 | 39 ± 4 |
| **Zr** | 402 | 435 | 420 | 397 | 486 ± 22 |
| **Nb** | 13.1 | 13.7 | 14.8 | 11.8 | 15 ± 2 |
| **Cs** | 18.0 | 17.8 | 18.3 | 17.4 | 18 ± 2 |
| **Ba** | 789 | 786 | 741 | 1410 | 834 ± 44 |
| **La** | 33.9 | 35.5 | 30.8 | 35.2 | 41 ± 5 |
| **Ce** | 73.2 | 74.5 | 69.4 | 77.6 | 86 ± 9 |
| **Pr** | 8.3 | 9.2 | 8.0 | 8.2 | 9 ± 1 |
| **Nd** | 32.1 | 31.3 | 29.3 | 29.7 | 37 ± 4 |
| **Sm** | 7.0 | 7.8 | 5.7 | 9.1 | 8 ± 2 |
| **Eu** | 0.5 | 0.6 | 0.7 | 1.0 | 1 ± 0.5 |
| **Gd** | 7.5 | 7.6 | 3.7 | 8.5 | 8 ± 3 |
| **Tb** | 0.9 | 0.7 | 0.6 | 1.2 | 1 ± 0.2 |
| **Dy** | 6.6 | 4.9 | 5.8 | 5.3 | 6 ± 2 |
| **Ho** | 1.4 | 1.0 | 0.6 | 1.0 | 1 ± 0.2 |
| **Er** | 3.6 | 2.8 | 2.9 | 2.5 | 4 ± 1 |
| **Tm** | 0.7 | 0.5 | 0.7 | 0.2 | 0.5 ± 0.3 |
| **Yb** | 2.6 | 2.9 | 2.2 | 4.2 | 4 ± 1.5 |
| **Lu** | 0.4 | 0.5 | 0.3 | 0.3 | 0.5 ± 0.2 |
| **Hf** | 12.2 | 12.4 | 11.9 | 11.8 | 14 ± 3 |

1056

1057 Notes. Values are in ppm. Sample prefixes are: X = xenolith glass; IG = interstitial glass. X2-
1058 1 and X2-2 are analyses on different spots from the same xenolith. Average values ± 2 s.d.
1059 compositional variability are shown for 7 analyses from IG12.

1060

1061

1062

1063

1064

1065

## FIGURE CAPTIONS

**Figure 1.** Location of the Taupo Volcanic Zone (TVZ) and associated features within the North Island of New Zealand. TVZ basement rock outcrops for the Torlesse and Waipapa terranes have been modified from Price et al. (2015). Locations for features referred to in the text are shown for White Island (WI), Kakuki basalt (K), Taupo volcano (TV), Waimarino basalt (W), Pukeonake (P), Tongariro (T), Hauhangatahi (H), Ruapehu (R) and Ohakune craters (O).

**Figure 2.** Geological map of chronostratigraphic formations at Ruapehu, modified from Conway et al. (2016). Marginal ticks and numbers are those of the NZTM 2000 grid, in meters; a reference point for latitude and longitude is marked in the top right of the map.

**Figure 3.** Petrographic features of representative Ruapehu lava flows. Red numbers indicate Mg# ([100Mg/(Mg + Fe)]) of EPMA spots. (a) Clinopyroxene in Te Herenga Formation basaltic-andesite sample CC348. (b) Cluster of zoned plagioclase crystals in Whakapapa Formation andesite sample CC281. (c) Reverse-zoned orthopyroxene in Mangawhero Formation (Mangaehuehu package) andesite sample CC077. (d) Cluster of reverse-zoned orthopyroxene crystals in Mangawhero Formation (Mangaehuehu package) andesite sample CC089. (e) Resorbed olivine crystal, with symplectite of magnetite (mt) and orthopyroxene overgrowth, in Whakapapa Formation sample CC335. (f) Quenched glass (gl) in fragment of feldspathic xenolith (plag) within Mangawhero Formation (Te Kohatu package) dacite sample CC415. For sample details and locations, see Conway (2016).

**Figure 4.** Bivariate plots of whole-rock $K_2O$, $Al_2O_3$, MgO, Ni, Rb and Zr versus $SiO_2$. Values of 2 s.d. uncertainty from XRF and ICP-MS analyses are smaller than the size of the symbols. Sample and standard data are in the Electronic Supplementary Material. Abbreviations for end-member samples referred to in the text are Te Kohatu package, high-K

dacite (TK), Whakapapaiti package, low-K dacite (WH) and Mangaehuehu package, high-MgO andesite (ME). Gray dots are data from Price et al. (2012). Type 2 plagioclase-phyric andesites of the Wahianoa Formation (Graham and Hackett, 1987) are the green diamonds labelled T2. Lines of best fit have been drawn in panel (a) and its inset plot to show the distinct trends for 50–35 ka lavas compared to <26 lavas. Arrows point towards representative mineral compositions to indicate azimuths of crystal accumulation (opposite direction indicates fractionation).

**Figure 5.** Whole-rock compositional characteristics (a) and spatial distribution (b) of early Mangawhero Formation lava flows. (a) MgO and versus $SiO_2$ plot for lavas erupted from 50–35 ka. Colour key for lava packages is shown in (b). Shaded fields show compositional ranges for pre-80 ka Ruapehu lavas (i), post-35 ka Ruapehu lavas (ii), and the ~26 ka Whakapapaiti dacite package (WH). Lines of best fit (dashed) for the low- and high-MgO suites are extended towards possible mafic end-members K (Kakuki basalt) and W (Waimarino basalt): basalt compositions are from Gamble et al. (1993). Average compositions of P (Pukeonake andesite) and O (Ohakune andesite) shown for comparison; data are from Cole (1978) and Hackett (1985). Locations of P and O are labelled in (b).

**Figure 6.** Time-composition relationships for Ruapehu lavas (after Conway et al. 2016). Lava ages are $^{40}Ar/^{39}Ar$ weighted mean plateau ages (WMPA) with associated 2 s.d. uncertainties shown by bars. Both ages and whole-rock compositions were determined for the same sample. The timing of the onset of deglaciation (light grey bar) and the sector collapse of the northern flank (dark grey bar) are shown on each panel. Data are also shown for lavas dated by Gamble et al. (2003) and lava clasts by Tost and Cronin (2015). Geochemical data for lava clasts is from Tost et al. (2016).

**Figure 7.** Multielement diagrams for Ruapehu lavas. Whole-rock trace element concentrations are normalised to average values of continental crust from Rudnick and Gao (2003). Grey line repeated in all panels is Te Herenga basaltic-andesite sample CC348. Approximate eruption age is labelled for each sample.

**Figure 8.** Whole-rock $^{143}Nd/^{144}Nd$ and $^{87}Sr/^{86}Sr$ isotopic compositions and $SiO_2$ contents for Ruapehu lavas with the samples allocated to the formations and age data from Conway et al. (2016). Isotopic data from Price et al. (2012). Note that 50–35 ka lavas with highest $^{87}Sr/^{86}Sr$ values do not appear in (a) because they do not have Nd isotopic data.

**Figure 9.** $SiO_2$-$K_2O$ compositional variations for whole-rock and glass compositions for Ruapehu lavas. Symbols are compositions for whole-rock (wr: coloured diamonds), melt inclusions (mi: open diamonds), groundmass glass (gm: coloured crosses) and xenolith glass (xg: open blue circles). Data are in the Electronic Supplementary Material. Fields are shown for Taupo volcano glass, post-Oruanui (TV) based on data from Barker et al. (2015), and pyroclast glass from post-glacial Ruapehu Plinian eruptions (RP) based on data from Pardo et al. (2014). Lines of best fit are shown for whole-rock data.

**Figure 10.** Plot of Rb/Zr variation with La/Sm for whole-rock lavas compared against inferred chemical evolution pathways (dotted lines, 10 % increments of fractionation). Trajectories represent AFC models for Ruapehu magmas using lava samples CC125 and GL1030 as starting compositions for 50-35 ka and <26 ka lavas, respectively. Following Price et al. (2012), a fractionating assemblage of plagioclase (0.59), clinopyroxene (0.25), orthopyroxene (0.16) was used to constrain bulk distribution coefficients (D) of 0.04 (Rb), 0.38 (Zr), 0.11 (La) and 0.29 (Sm) that were calculated using the values available at the Earth Reference Data and Models website (EarthRef: http://www.earthref.org), as collated in the Electronic Supplementary Material. High-K (6 wt. % $K_2O$) and low-K (4 wt. % $K_2O$) crustal

assimilants with corresponding ratios of assimilation to fractionation (R) of 0.5 and 0.25 were used. The trace element compositions of the assimilant were constrained by analyses of xenolith glass from metasedimentary fragments within a 40 ka dacite lava (this study; CC415-X2) and within a Whakapapa Formation lava (Price et al. 2005; 104x). Modelling was performed using the PetroGraph software program (Petrelli et al. 2005). See text for discussion.

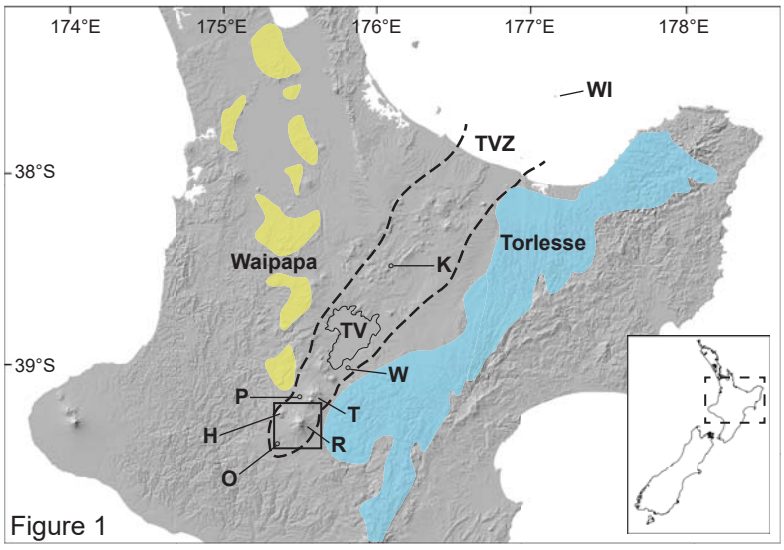
174°E
175°E
176°E
177°E
178°E
38°S
39°S
WI
TVZ
Torlesse
Waipapa
K
TV
W
P
T
H
R
O

Figure 1

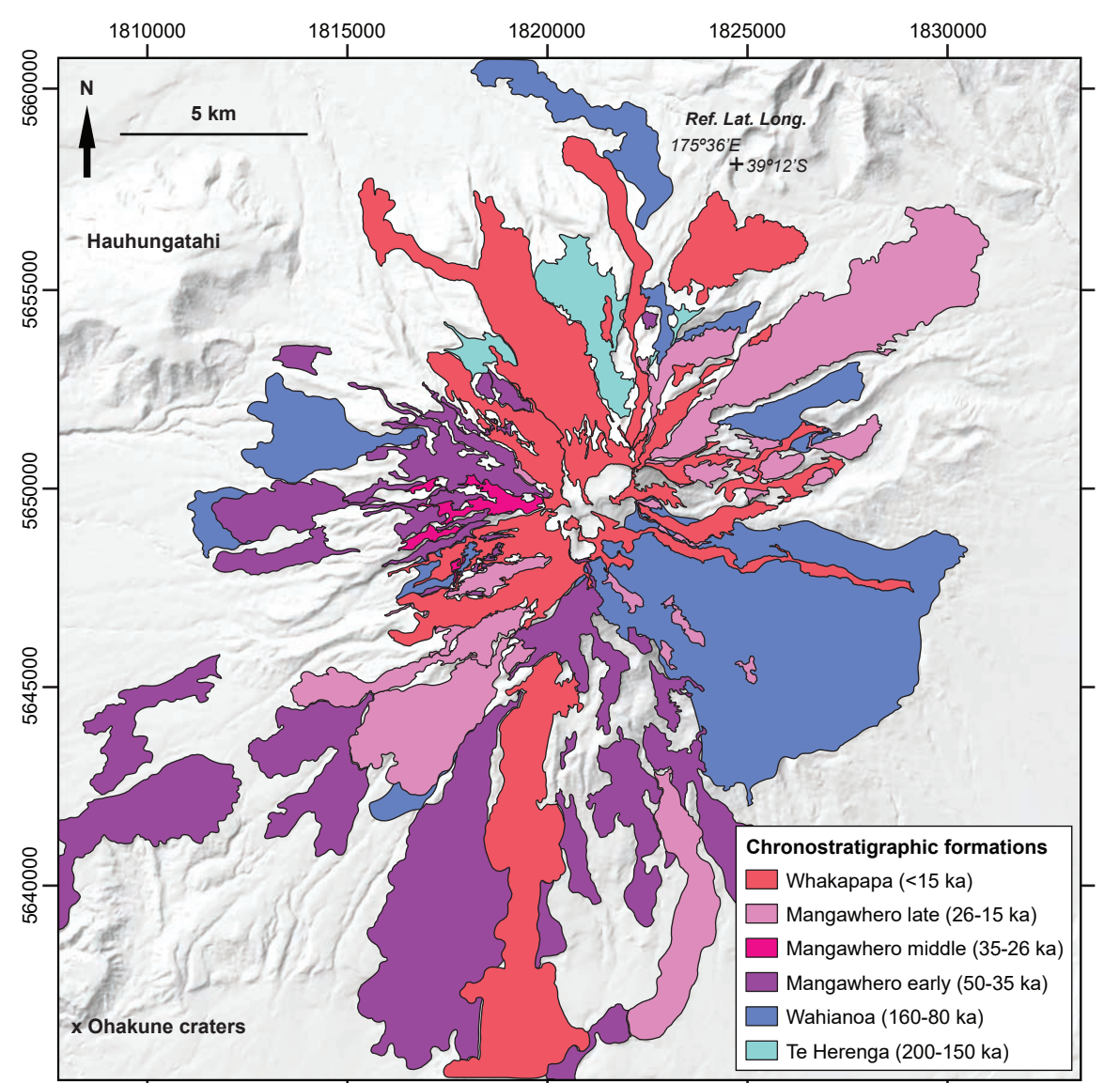
1810000
1815000
1820000
1825000
1830000
5660000
5655000
5650000
5645000
5640000
N
5 km
Ref. Lat. Long.
175°36'E
39°12'S
Hauhungatahi
x Ohakune craters
Chronostratigraphic formations
Whakapapa (<15 ka)
Mangawhero late (26-15 ka)
Mangawhero middle (35-26 ka)
Mangawhero early (50-35 ka)
Wahianoa (160-80 ka)
Te Herenga (200-150 ka)

Figure 2

Figure 3

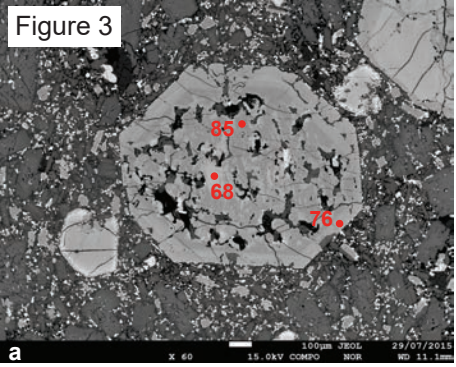
85
68
76
a
x 60
100µm JEOL
15.0kV COMPO NOR
29/07/2015
WD 11.1mm

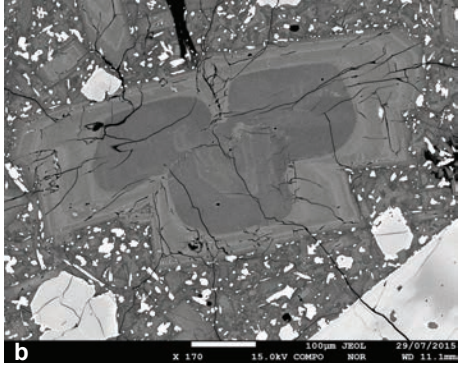
b
x 170
100µm JEOL
15.0kV COMPO NOR
29/07/2015
WD 11.1mm

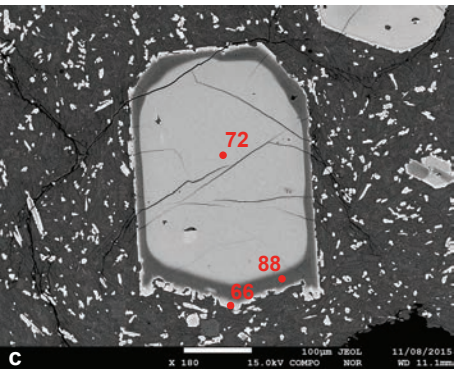
72
88
66
c
x 180
100µm JEOL
15.0kV COMPO NOR
11/08/2015
WD 11.1mm

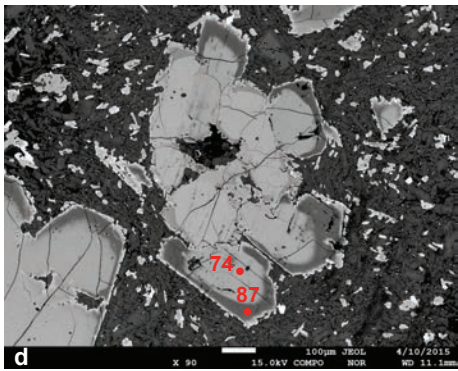
74
87
d
x 90
100µm JEOL
15.0kV COMPO NOR
4/10/2015
WD 11.1mm

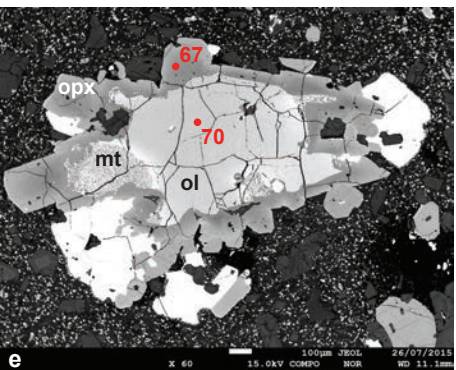
67
opx
70
mt
ol
e
x 60
100µm JEOL
15.0kV COMPO NOR
26/07/2015
WD 11.1mm

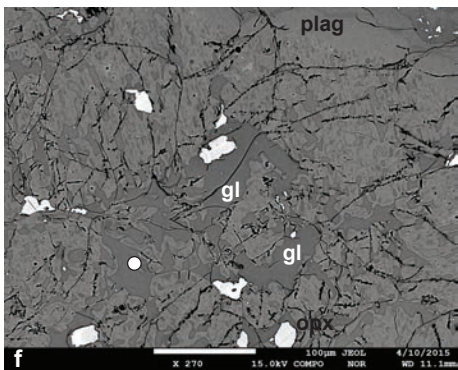
plag
gl
gl
opx
f
x 270
100µm JEOL
15.0kV COMPO NOR
4/10/2015
WD 11.1mm

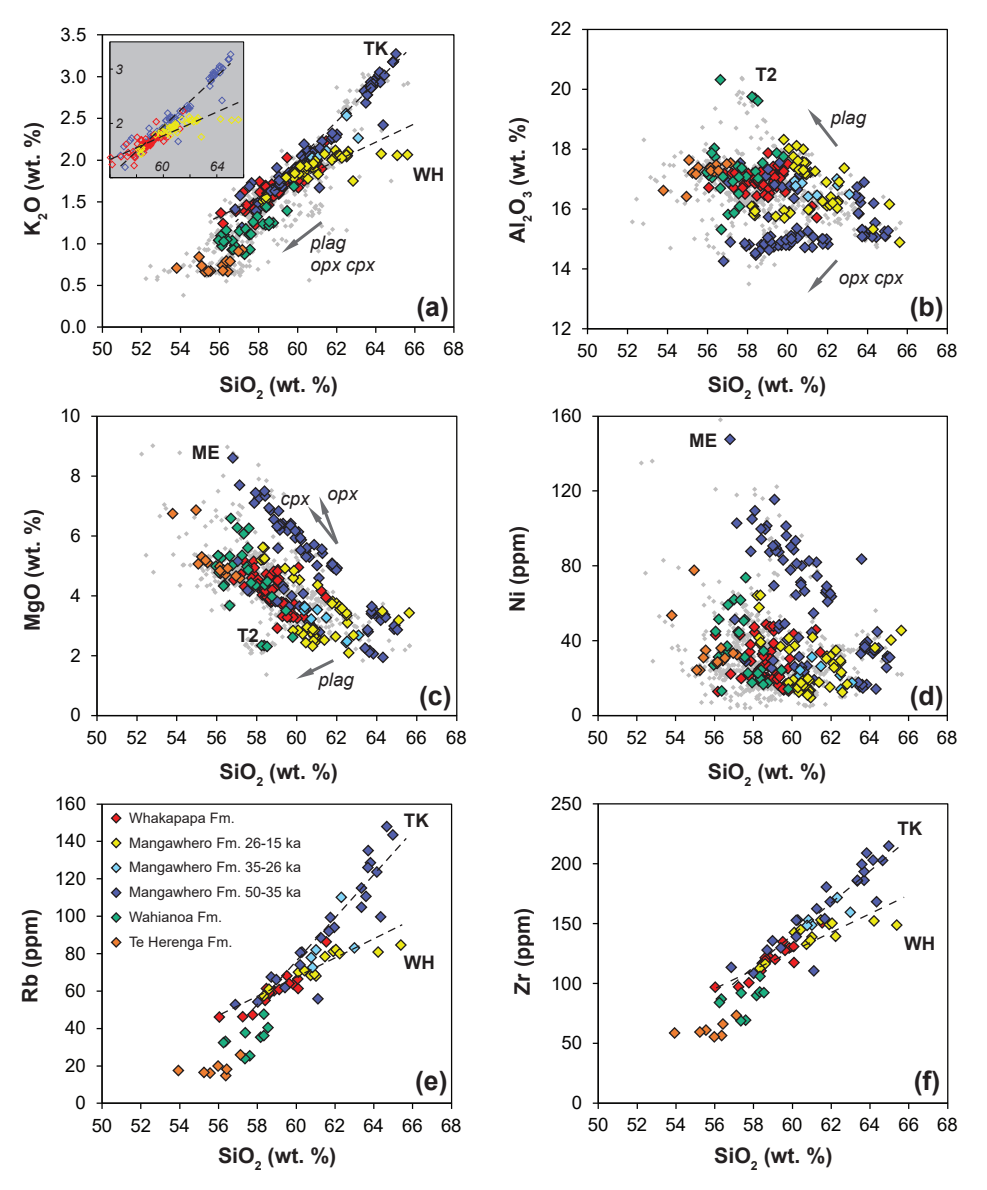
K2O (wt. %)
SiO2 (wt. %)
TK
WH
plag
opx cpx
(a)
Al2O3 (wt. %)
T2
plag
opx cpx
(b)
MgO (wt. %)
ME
cpx
opx
T2
plag
(c)
Ni (ppm)
ME
(d)
Rb (ppm)
Whakapapa Fm.
Mangawhero Fm. 26-15 ka
Mangawhero Fm. 35-26 ka
Mangawhero Fm. 50-35 ka
Wahianoa Fm.
Te Herenga Fm.
TK
WH
(e)
Zr (ppm)
TK
WH
(f)

Figure 5

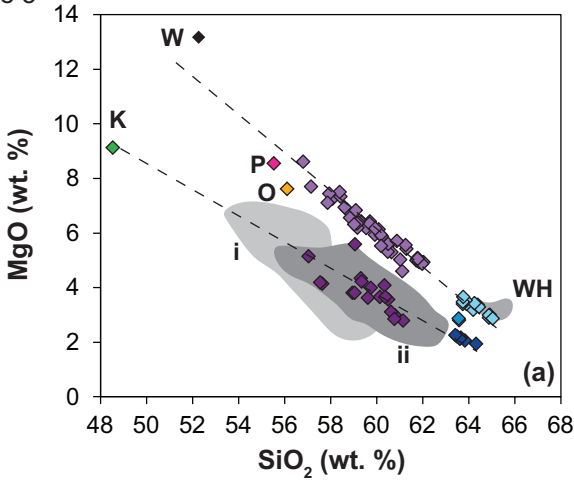
W
K
P
O
i
ii
WH
(a)
MgO (wt. %)
SiO2 (wt. %)
0
2
4
6
8
10
12
14
48
50
52
54
56
58
60
62
64
66
68

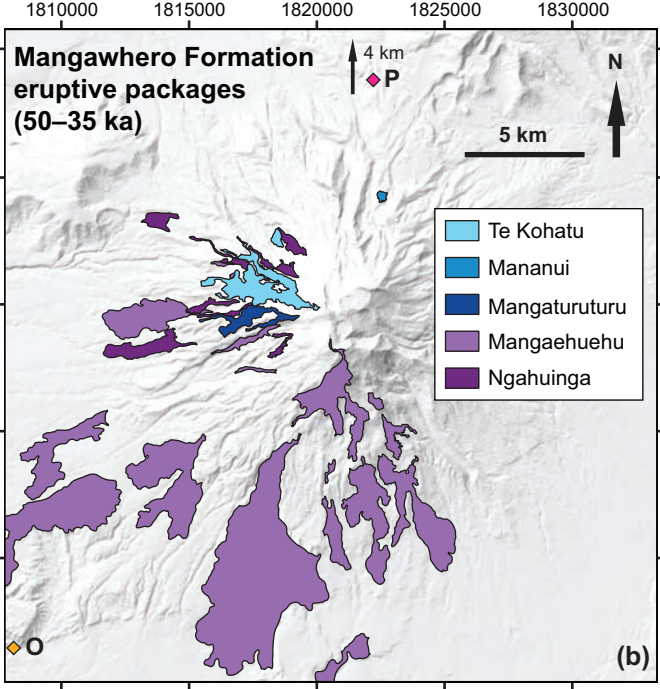
Mangawhero Formation
eruptive packages
(50–35 ka)
4 km
P
5 km
N
Te Kohatu
Mananui
Mangaturuturu
Mangaehuehu
Ngahuinga
O
(b)
1810000
1815000
1820000
1825000
1830000
5660000
5655000
5650000
5645000
5640000

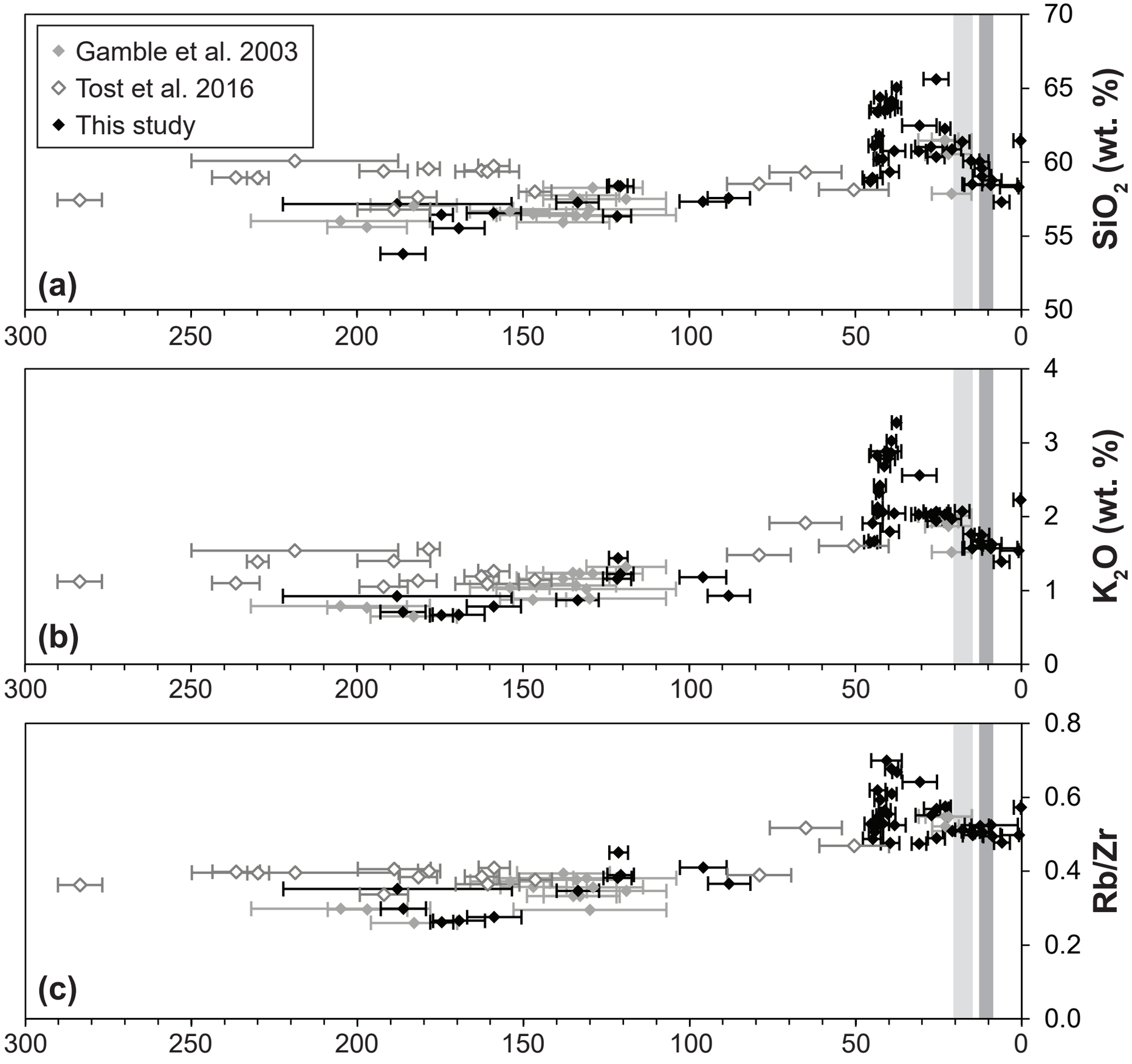
Gamble et al. 2003
Tost et al. 2016
This study
(a)
(b)
(c)
SiO2 (wt. %)
K2O (wt. %)
Rb/Zr
70
65
60
55
50
4
3
2
1
0
0.8
0.6
0.4
0.2
0.0
300
250
200
150
100
50
0
40Ar/39Ar age (ka)

Figure 6

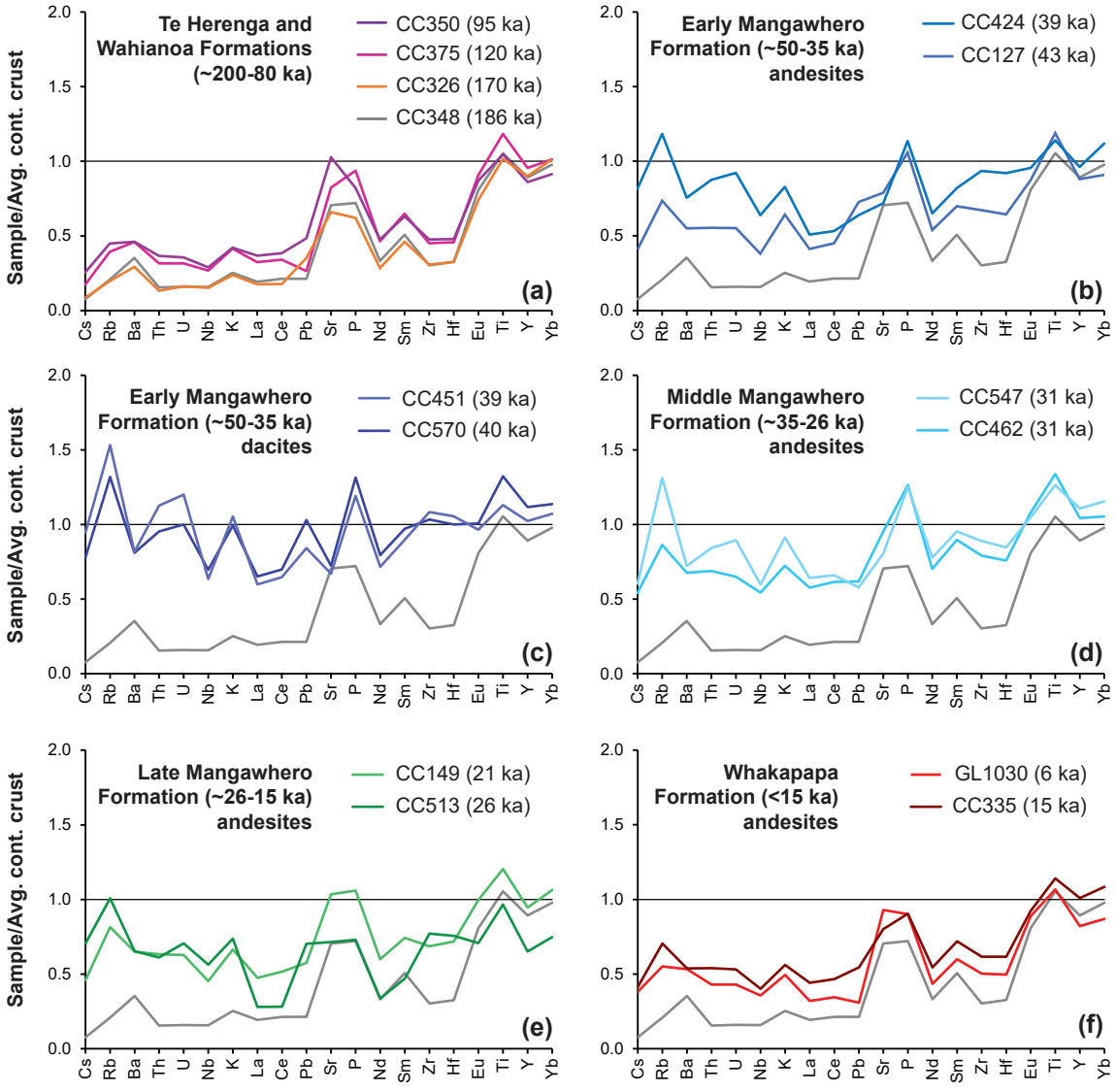
Te Herenga and Wahianoa Formations (~200-80 ka)
CC350 (95 ka)
CC375 (120 ka)
CC326 (170 ka)
CC348 (186 ka)
(a)
Early Mangawhero Formation (~50-35 ka) andesites
CC424 (39 ka)
CC127 (43 ka)
(b)
Early Mangawhero Formation (~50-35 ka) dacites
CC451 (39 ka)
CC570 (40 ka)
(c)
Middle Mangawhero Formation (~35-26 ka) andesites
CC547 (31 ka)
CC462 (31 ka)
(d)
Late Mangawhero Formation (~26-15 ka) andesites
CC149 (21 ka)
CC513 (26 ka)
(e)
Whakapapa Formation (<15 ka) andesites
GL1030 (6 ka)
CC335 (15 ka)
(f)
Sample/Avg. cont. crust
2.0
1.5
1.0
0.5
0.0
Cs Rb Ba Th U Nb K La Ce Pb Sr P Nd Sm Zr Hf Eu Ti Y Yb
Element

Figure 7

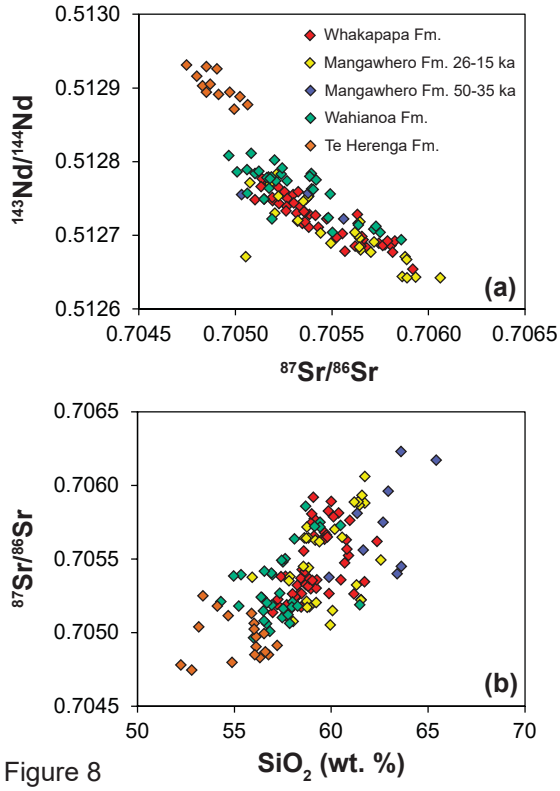
0.5130
0.5129
0.5128
0.5127
0.5126
143Nd/144Nd
Whakapapa Fm.
Mangawhero Fm. 26-15 ka
Mangawhero Fm. 50-35 ka
Wahianoa Fm.
Te Herenga Fm.
(a)
0.7045
0.7050
0.7055
0.7060
0.7065
87Sr/86Sr
0.7065
0.7060
0.7055
0.7050
0.7045
87Sr/86Sr
(b)
50
55
60
65
70
SiO2 (wt. %)

Figure 8

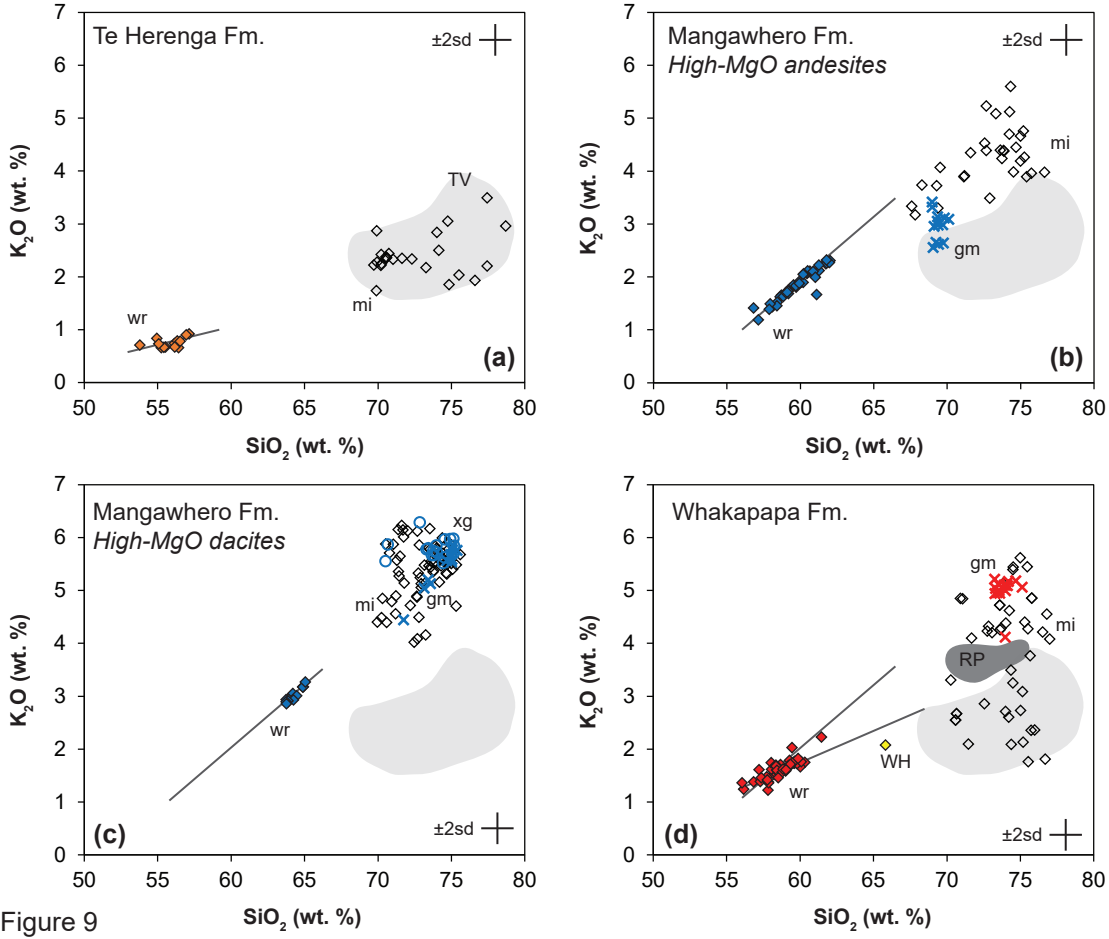
Te Herenga Fm.
±2sd
TV
mi
wr
(a)
Mangawhero Fm.
High-MgO andesites
±2sd
mi
gm
wr
(b)
Mangawhero Fm.
High-MgO dacites
xg
mi
gm
wr
(c)
±2sd
Whakapapa Fm.
gm
mi
RP
WH
wr
(d)
±2sd
K2O (wt. %)
SiO2 (wt. %)

Figure 9

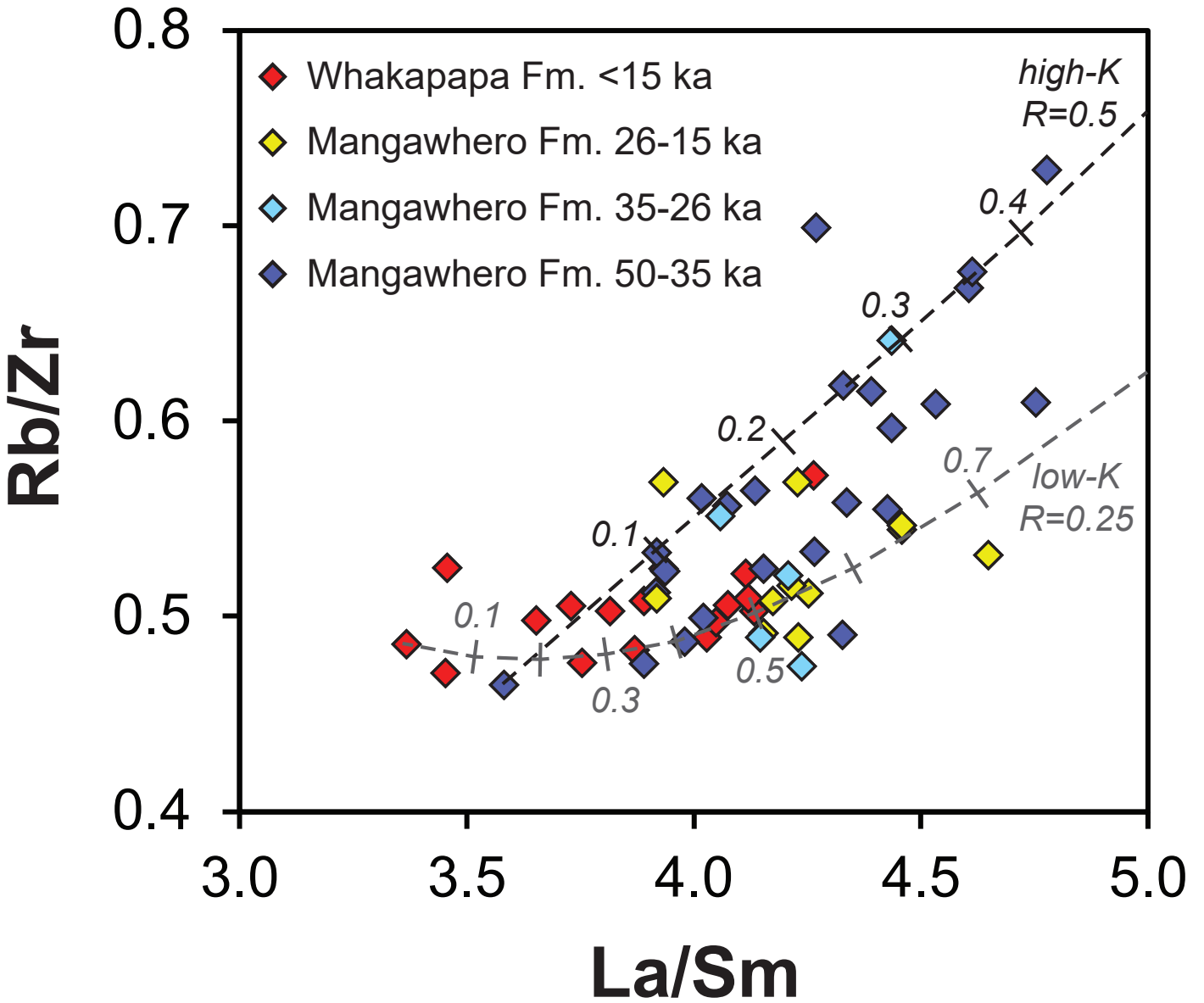
Whakapapa Fm. <15 ka
Mangawhero Fm. 26-15 ka
Mangawhero Fm. 35-26 ka
Mangawhero Fm. 50-35 ka
high-K
R=0.5
low-K
R=0.25
0.1
0.2
0.3
0.4
0.7
0.1
0.3
0.5
0.8
0.7
0.6
0.5
0.4
Rb/Zr
3.0
3.5
4.0
4.5
5.0
La/Sm